

## **Connexins are essential for the contribution of latent progenitors to self-repair after spinal cord injury**

María Victoria Falco<sup>\*1</sup>, Gabriela Fabbiani<sup>\*1</sup>, Daniel Prieto<sup>1</sup>, Mateo Vidal<sup>1</sup>, Milagros Benítez<sup>1</sup>, María Inés Rehermann<sup>1</sup>, Constanza Silvera<sup>1</sup>, Renata Simeone<sup>1</sup>, Federico F. Trigo<sup>2</sup>, Raúl E. Russo<sup>1,#</sup>

<sup>1</sup>Departamento de Neurofisiología Celular y Molecular, <sup>2</sup>Departamento de Señalización Glial y Neuronal, Instituto de Investigaciones Biológicas Clemente Estable. Avenida Italia 3318, CP11600 Montevideo, Uruguay.

\* These authors contributed equally to this work.

**Running title:** connexins regulate the response of ependymal cells to injury

Keywords: spinal cord injury, neural stem cells, connexin 26, connexin 43, neural regeneration, calcium waves

### **#Corresponding author:**

Dr. Raúl E. Russo

Neurofisiología Celular y Molecular  
Instituto de Investigaciones Biológicas  
Clemente Estable  
Avenida Italia 3318  
CP 11600, Montevideo  
Uruguay  
Tel.: (5982) 487 5532  
Fax: (5982) 487 5548  
e-mail: [rrusso@iibce.edu.uy](mailto:rrusso@iibce.edu.uy)  
[russoblanc@gmail.com](mailto:russoblanc@gmail.com)

**Conflict of interests:** The authors declare no competing financial interests.

### **Acknowledgments**

We would like to thank Dr. Jonas Frisén for the generous gift of the FoxJ1CreER-tdTomato transgenic mouse. We thank Tabaré de los Campos for developing a macro to quantify connexin puncta. This work was supported by the Wings for Life, Spinal Cord Research Foundation (WFL-UY-13/23 Project #290), the Morton Cure Paralysis Fund and CSIC (grant #881412) to RER, and

by the Agencia Nacional de Investigación e Innovación (ANII, grant FCE\_3\_2022\_1\_172524) to GF. MVF was supported by ANII.

## Abstract

Gap junctions are important regulators of the biology of neural stem cells. Both in vertebrates with regenerative abilities and neonatal rodents, ependymal cells communicate via connexin (Cx) 43 and Cx26. Gap junction coupling and Cx26 are down-regulated as the ependyma becomes quiescent in adulthood, but injury overrules this developmental down-regulation suggesting a role for Cx signalling in the reactivation of ependymal cells. Here, we aim to explore the role of Cx26 and Cx43 in the response of ependymal cells to injury. We find that Cx26 is critical for the proliferative response to injury and thereby scar formation. Cx43 plays a key role in the communication between ependymal cells of  $Ca^{2+}$  signals induced by activation of P2X7 receptors that trigger downstream events. Our data show that Cxs are relevant targets to manipulate the ependymal stem cell niche to achieve a better self-repair after spinal cord injury.

## Main

The traumatic injury of the spinal cord (SC) leads to devastating conditions because of the disruption of axonal pathways, neuronal death, axonal demyelination and scarring<sup>1</sup>. Although mammals lack the ability for self-repair displayed by some non-mammalian vertebrates<sup>2</sup>, some cells in the ependyma still react to injury generating new cells that migrate towards the lesion to become astrocytes within the core of the scar<sup>3,4</sup>. The manipulation of ependymal cells is regarded as a promising strategy to potentiate healing<sup>5</sup>. To unleash the regenerative potential of the ependymal stem cell niche, a better understanding of the mechanisms that reactivate these dormant progenitor-like cells after injury is needed.

Gap junction coupling has an important role in the regulation of neural stem cells<sup>6</sup>, with connexin (Cx) 43 and Cx26 expressed in radial glia during cortical development<sup>7,8</sup>. The role of Cxs as regulators of proliferation is maintained in adult neurogenic niches<sup>9</sup>. Both in vertebrates with regenerative abilities and in neonatal rodents, ependymal cells in the SC communicate via Cx43 and Cx26<sup>10,11</sup>. The incidence of gap junction coupling is developmentally down-regulated as the ependyma becomes quiescent in adulthood, an event paralleled by downregulation of Cx26<sup>12</sup>. At the time injury-induced proliferation peaks<sup>3</sup>, gap junction coupling between ependymal cells increases, resembling the functional state of the immature ependyma<sup>12</sup>. Interestingly, injury overrules the developmental down-regulation of Cx26 in ependymal cells suggesting a role in the awakening of these latent progenitors.

Cx signalling is important for wound healing and scarring in different types of tissues<sup>13</sup>. The idea that Cxs play a similar function in the ependymal stem cell niche to regulate self-repair is supported by the fact that pharmacological blockade of gap junctions reduced injury-induced proliferation of ependymal cells<sup>12</sup>. In epithelia, the wound-induced changes of Cx26 and Cx43 expression occur in a complex spatiotemporal manner<sup>14</sup> and the blockade of Cx43 speeds up wound closure<sup>15</sup>. We speculated that Cx26 and Cx43 may play a similar role in self-repair mediated by ependymal cells. Here, we aimed to explore the role of Cx26 and Cx43 in the response of ependymal cells to injury. We used a Cre-Lox system to specifically delete Cx26 or Cx43 in ependymal cells. By applying a multi-technical approach in vivo and in vitro, we find that injury-induced expression of Cx26 is critical for the proliferative response of ependymal cells to injury, and its absence generates a severe impairment of scar formation. On the other hand, Cx43 participates in the early cellular signalling of injury and its deletion also reduces the response of the ependyma to traumatic injury. Our data suggests that Cx43 -together with P2X7receptors- plays a key role in the communication between ependymal cells via Ca<sup>2+</sup> waves that trigger

downstream events such as the Cx26 up-regulation needed for the resumption of proliferation. Collectively, our data support the idea that Cxs are key regulators of the biology of dormant progenitor-like cells and represent relevant targets to improve the response of the ependymal stem cell niche to promote a better self-repair after spinal cord injury (SCI).

## Results

Gap junction coupling and Cx26 expression decline during post-natal development as the ependymal stem cell niche becomes quiescent in adulthood<sup>12</sup>. SCI induces a strong reactivation of progenitor-like cells in the ependyma that is paralleled by the re-expression of Cx26 and an increased incidence of gap junction coupled cells, suggesting Cx26 may be implicated in the mechanisms involved in re-entering the cell cycle. Indeed, the pharmacological blockade of gap junctions and Cx hemichannels with the peptide Gap26 strongly reduces the injury-induced proliferation of ependymal cells<sup>12</sup>. However, this pharmacological approach has the limitation that Gap26 blocks all types of Cxs in different types of cells within the SC. To tackle the role of specific Cx isoforms in ependymal cells, we used a Cre-Lox system to genetically delete Cx26 selectively in ependymal cells by crossing FoxJ1CreER-tdT -which expresses the Cre recombinase under the control of the FoxJ1 promoter active in cells with motile cilia<sup>4,16</sup>- with mice having the Cx26 gene (GJB2) between LoxP sites (Fig. 1 a). We induced recombination in FoxJ1CreER-tdT-Cx26<sup>fl/fl</sup> mice by injection of tamoxifen during 5 days and let 10 days for tamoxifen clearance to perform a dorsal hemisection of the SC (Fig. 1 b). As described before<sup>12</sup>, injury induced a robust expression of Cx26 in control mice (Fig. 1 c,d). We found that recombination in Cx26<sup>fl/fl</sup> mice significantly reduced the expression of Cx26 induced by injury in the ependyma (Fig. 1 e-g,  $p < 0.0001$ , Mann-Whitney U test). The number of Cx26 puncta outside the ependyma was similar in control and Cx26<sup>-/-</sup> mice at 5 DPI (Extended Data Fig. 1 a, b-d,f;  $p = 0.45$ , Kruskal-Wallis multiple comparisons test), showing that the deletion of Cx26 was selective for ependymal cells. We next used a proliferation assay by injecting the thymidine analogue EdU from day 2 to 5 after SCI (Fig. 1 b) to test whether the deletion of Cx26 in ependymal cells affected the proliferative reaction of ependymal cells to injury. We found that the number of Edu+ nuclei within the ependyma at 5 DPI -a time at which the injury-induced proliferation peaks- was significantly reduced in Cx26<sup>-/-</sup> mice compared to FoxJ1CreER-tdT control animals (Fig. 1 h-l,  $p < 0.0001$ , Mann-Whitney U test).

Various neurotransmitters regulate the biology of ependymal cells<sup>17-20</sup>. ATP is massively released after SCI<sup>21</sup> and the activation of P2X7 receptors (P2X7r) in ependymal cells leads to the resumption of proliferation in a way similar to that induced by injury<sup>22</sup>. To explore whether Cx26 is involved in the reactivation of dormant ependymal cells induced by P2X7r activation, we injected the selective P2X7r agonist BzATP (1 mM, 1  $\mu$ l) close to the central canal (CC) (Fig. 2 a). We compared the proliferation induced by P2X7r activation in FoxJ1CreER-tdT control animals and that of Cx26<sup>-/-</sup>. The rate of proliferation in the intact adult ependyma is very low<sup>3,4,23</sup> but increases substantially after activation of P2X7r by BzATP injection<sup>22</sup>. Figure 2 b-d shows that

BzATP injection close to the CC in control FoxJ1CreER-tdT mice induced ependymal cell proliferation as evidenced by EdU uptake. However, genetic deletion of Cx26 strongly reduced the reactivation of ependymal cell proliferation induced by P2X7r activation (Fig. 2 e-g). Figure 2 h shows the spatial profile of EdU uptake around BzATP injection. The analysis of the number of EdU+ nuclei in  $\pm 500 \mu\text{m}$  around the injection site shows a significant difference in EdU+ nuclei between control and Cx26<sup>-/-</sup> mice (Fig. 2 i,  $p < 0.0001$ , Mann-Whitney U test). These data suggest that Cx26 also plays a key role in the molecular mechanisms triggered by activation of P2X7r to induce ependymal cell proliferation.

### **Cx43 also contributes to the response of ependymal cells to injury**

Unlike Cx26, the expression of Cx43 in ependymal cells close to the injury site does not change after injury<sup>12</sup>. Based on wound healing in other tissues<sup>24</sup>, we hypothesized that Cx43 might be detrimental for the response of ependymal cells to injury. To evaluate this possibility, we genetically deleted the Cx43 (GJA1) gene from ependymal cells using the same strategy as for Cx26 (Fig. 3 a,b). As described previously<sup>12</sup>, Cx43 is robustly expressed in the ependyma of the adult SC of FoxJ1CreER-tdT (Fig. 3 c,d). Recombination in FoxJ1CreER-tdT-Cx43<sup>fl/fl</sup> mice significantly reduced the number of Cx43 puncta within the ependyma (Fig. 3 e-g,  $p < 0.01$  Mann-Whitney U test). Surprisingly, we found that Cx43 deletion strongly reduced the proliferative reaction of the ependyma at 5 DPI (Fig. 3 h-i,  $p < 0.05$  Mann-Whitney U test). We wondered whether Cx26 was still being up-regulated by injury when Cx43 had been deleted, but was no longer efficient to promote ependymal cell proliferation. Immunohistochemistry for Cx26 in Cx43<sup>-/-</sup> mice at 5 DPI showed that in the absence of Cx43, injury did not trigger the expression of Cx26 needed to awake ependymal cells (Fig. 3 m-q,  $p < 0.05$  Mann-Whitney U test). The expression of Cx26 in the parenchyma outside the ependyma was not affected in Cx43<sup>-/-</sup> mice (Extended Data Fig. 1 c,e-f,  $p = 0.91$ , Kruskal-Wallis multiple comparisons test). The most parsimonious interpretation of these results is that the effect of Cx43 on injury-induced proliferation is indirect via the interference of the injury-induced Cx26 up-regulation.

### **Deletion of Cxs in ependymal cells impacts scar formation**

We next evaluated the impact of Cx deletion in ependymal cells on scar formation. As reported before<sup>4</sup>, in FoxJ1CreER-tdT mice the lesion site is filled with scar tissue and abundant ependyma-derived cells at 30 DPI (Fig. 4 a). Many tdT+ cells can be observed migrating away from the CC (Fig. 4 b). The area occupied by tdT+ cells over the total area of the cord at the lesion site remains about the same between 2- and 4-weeks post-injury, suggesting the number of ependyma-derived

cells correlates with the restoration of the damaged area (Fig. 4 c). We found that the lack of Cx26 up-regulation that normally occurs after injury and the interference it generated on injury-induced proliferation had a profound effect on the formation of the glial scar. After Cx26 deletion, fewer tdT+ cells could be observed away from the CC when compared to control (Fig. 4 d-e). Similar findings were obtained after deletion of Cx43 (Fig. 4 f). Cx26 deletion in ependymal cells impaired the contribution of the ependyma to scar formation around the lesion epicenter as evidenced by the measurement of the normalized area of the cord (Fig. 4 g-h;  $p < 0.05$ , One Way ANOVA Dunnett's multiple comparison test). Although the mean area of the cord around the lesion epicenter in Cx43<sup>-/-</sup> mice was smaller, there was not significant difference compared to control animals (Fig. 4 h,  $p = 0.53$ , One Way ANOVA Dunnett's multiple comparison test). Our results are similar to those obtained in mice after deletion of Ras genes in ependymal cells<sup>25</sup>, and confirm the importance of the latent ependymal stem cell niche for self-repair and the relevance of Cx signalling to support the ependymal cell response to injury.

### **Communication between ependymal cells by Cxs**

We were puzzled by the fact that Cx43 affects Cx26 expression and thereby the response of ependymal cells to SCI. We speculated that the impact of Cx43 deletion on the ependymal cell reaction may be by interference with the communication between ependymal cells. We took advantage that the immature ependyma is an active stem cell niche with robust gap junction coupling and expression of both Cx26 and Cx43 to explore the role of specific Cx isoforms in gap junction coupling. As already described for adults, we induced recombination of FoxJ1CreER-tdT-Cx26<sup>fl/fl</sup> and FoxJ1CreER-tdT-Cx43<sup>fl/fl</sup> in neonatal mice (two daily injections of tamoxifen at P9 and 10) to delete a selected Cx from ependymal cells (Extended Data Fig. 2). Patch clamp recordings of neonatal ependymal cells (P11) in control (FoxJ1CreER-tdT) animals revealed cells with passive properties (Fig. 5 a-b, control,  $n = 12$ ) whose input resistance increased after addition of the gap junction decoupler meclofenamic acid (MFA, 100  $\mu\text{M}$ ,  $n = 7$ ; Fig. 5 a-c;  $p < 0.05$  Wilcoxon Signed-Rank test), suggesting gap junction coupling between ependymal cells. In line with this, the diffusion of biocytin -a compound highly permeable through connexons- showed extensive dye coupling (Fig. 5 d). Deletion of Cx26 did not significantly change the input resistance of patch clamp recorded ependymal cells (Fig. 5 g,  $p = 0.97$ , Mann-Whitney Wilcoxon rank test) or the size of biocytin-labelled cells (Fig. 5 e, h;  $p > 0.99$ , Kruskal-Wallis multiple comparison test). In contrast, patch clamp recordings of Cx43<sup>-/-</sup>ependymal cells increased the apparent input resistance of cells (Fig. 5 g,  $p < 0.005$ , Mann-Whitney Wilcoxon rank test) and revealed either isolated cells (Fig. 5 f) or pauci-cellular clusters of coupled cells with significantly decreased cell cluster volumes (Fig. 5

h;  $p < 0.05$ , Kruskal-Wallis test). These data suggests that Cx43 is the main contributor to communication via gap junctions between ependymal cells.

Besides connexons forming gap junction plaques, there is a sub-population of permeable Cx43 hemichannels in the intact ependyma of the SC<sup>12</sup>. In line with this, the uptake of ethidium bromide in ependymal cells of Cx43<sup>-/-</sup> mice was strongly reduced compared to control FoxJ1CreER-tdT mice (Extended Data Fig. 3 a-e,  $p < 0.005$ , Mann-Whitney U test) and in recombined versus non-recombined cells in Cx43<sup>-/-</sup> (Extended Data Fig. 3 c-d,f,  $p < 0.05$ , Wilcoxon Signed-Rank test). We then asked whether the effect of Cx43 deletion on the injury-induced proliferation could be partly accounted by the absence of Cx43 hemichannels. To explore this possibility, we made a pre-emptive intraspinal injection of the Cx43 hemichannel blocker TAT-Gap19 (1 mM, 1  $\mu$ l) before a dorsal hemisection of the cord, followed immediately by filling the injury site with pluronic F127 gel embedded TAT-Gap19 (1 mM, Fig. 6 a). The application of the scrambled version of TAT-Gap19 peptide (Scr-TAT-Gap19) was used as control. We found that Scr-TAT-Gap19 did not affect the injury-induced proliferation (Fig. 6 b-c) but TAT-Gap19 reduced the number of EdU+ nuclei in ependymal cells in response to injury (Fig. 6 d-e). Figure 6 f shows the spatial profile of EdU+ nuclei around the lesion epicentre in TAT-Gap19 and Src-TAT-Gap19. The analysis of EdU+ nuclei in a  $\pm 500 \mu$ m extension around the lesion epicentre shows that TAT-Gap19 significantly reduced the injury-induced proliferation of ependymal cells (Fig. 6 g;  $p < 0.0001$  Mann-Whitney U test), suggesting Cx43 hemichannels are an important component of the early signalling needed to reactivate the latent ependymal progenitor-like cells.

Because Cx43 is expressed in the ependymal cells of the uninjured SC, we speculated that Cx43 may play a part in the earliest events taking place after injury by regulating communication between ependymal cells and Ca<sup>2+</sup> signals triggered by P2X7r activation<sup>26</sup>. To evaluate this possibility, we crossed FoxJ1CreER with Gt(ROSA)26Sortm38(CAG-GCaMP3)Hze/J mice to express GCaMP3 -a Ca<sup>2+</sup> sensing protein- in ependymal cells and made spinal cord slices from adult animals. Puff application of BzATP in a discrete region of the CC (Fig. 7 a1) induced Ca<sup>2+</sup> waves that propagated within the ependyma (Fig. 7 a3-4, b). In some regions of interest (ROI), secondary waves appeared at longer delays (Fig. 7 b, asterisks). Figure 7 c shows at a faster time scale that the Ca<sup>2+</sup> wave initiated and peaked earlier in some ROI, suggesting a propagation from leading to follower cells within the ependyma (Supplementary Information Video 1). The gap junction decoupler MFA spared the earliest component but strongly reduced the delayed peak of the Ca<sup>2+</sup> wave (Fig. 7 d-e). The propagation of the wave measured as the number of ROI in which  $\Delta F/F_0$  crossed a threshold ( $F_0$  mean + 8 SD before BzATP) decreased significantly after addition

of MFA (100  $\mu$ M; Fig. 7 f,  $p < 0.01$ , Wilcoxon Signed-Rank test; Supplementary Information Video 2). The comparison of the  $\text{Ca}^{2+}$  wave propagation among ependymal cells in slices incubated in normal Ringer's solution and MFA (100  $\mu$ M) showed a similar result (Fig. 7 g,  $p < 0.005$ , Mann-Whitney U test) and an overall decrease of the maximal  $\Delta F/\text{Fo}$  of different ROI (Fig. 7 h,  $p < 0.0001$  Mann-Whitney U test). Because MFA blocks both gap junctions and Cx hemichannels, we explored the effects of the hemichannel blocker TAT-Gap19 on  $\text{Ca}^{2+}$  signals triggered by P2X7r activation. Although the mean ratio of active ROI/total ROI was lower in TAT-Gap19 compared to the scrambled version of the peptide, there was no statistically significant difference (Fig. 7 i,  $p = 0.5009$ , Mann-Whitney U test). However, TAT-Gap19 significantly reduced the peak  $\Delta F/\text{Fo}$  in the total ROI analysed (Fig. 7 j,  $p < 0.0001$ , Mann-Whitney U test).

Although we cannot exclude non-canonical functions of Cx43, our data suggests that Cx43 - probably via gap junction and hemichannels- is important for the communication of  $\text{Ca}^{2+}$  signals initiated by activation of P2X7r by ATP released by tissue damage, blocking downstream events such as the expression of Cx26 that seems critical for the resumption of ependymal cell proliferation.

## Discussion

Endogenous latent progenitor-like cells in the ependyma are a potential source for improving self-repair and functional recovery after SCI<sup>5</sup>. To optimize the potential of the ependymal stem cell niche for repair, understanding the mechanisms by which progenitors are reactivated by injury is fundamental. Cx's play key roles in the regulation of the biology of stem cells and in wound healing in different tissues. Here, we show that Cx26 and Cx43 are needed for the reaction of ependymal cells to injury, and their lack has profound implications for endogenous repair.

Different isoforms of Cx's are dynamically expressed from the earliest embryonic developmental stages and regulate events such as proliferation, migration and differentiation of neural progenitors<sup>27</sup>. In particular, Cx43 and Cx26 appear in specific time and spatial domains in the cortical plate of mice, regulating the proliferation of radial glia and the migration of newborn neurons<sup>7,8</sup>. The importance of Cx's is maintained in adult neurogenic niches as knockout of Cx30 and Cx43 in progenitors of the dentate gyrus decreases their proliferation<sup>9</sup>. Both Cx43 and Cx26 are expressed in ependymo-radial glia of the spinal cord of the turtle, a vertebrate with remarkable self-repair capabilities<sup>10,28</sup>. Similarly, the active ependymal stem cell niche of neonatal mice has a robust expression of Cx26 and Cx43 with a prominent electrical and metabolic communication via gap junctions, suggesting that Cx signalling in the ependyma shares mechanisms with bona fide stem cell niches of the developing mammalian brain<sup>8,29,30</sup>. As postnatal development proceeds and the ependyma becomes quiescent, gap junction coupling and Cx26 declines, whereas Cx43 expression revealed by immunohistochemistry, remains unchanged. Gap junction coupling and Cx26 expression increases around the lesion epicentre at the time injury-induced proliferation peaks, suggesting a role for Cx26 in the resumption of the mitotic activity of ependymal cells<sup>12</sup>. In line with this, we find here that selective genetic deletion of Cx26 in ependymal cells dramatically reduced the proliferative reaction of the ependymal stem cell niche to injury. The reduced number of ependyma-derived cells had a profound effect on scar formation. Our results resemble those of Sabelström et al. (2013)<sup>25</sup> obtained by deletion of Ras genes and support the idea that the contribution of the ependymal stem cell niche is fundamental for scar formation and the limitation of tissue damage. Cx26 and Cx43 are differentially expressed during the cell cycle of murine neocortical precursors, with Cx26 increasing in mitotic cells between the S and early G1 phases<sup>7,8</sup>. In line with this, and given that Cx43 expression in ependymal cells around the lesion epicentre does not change after injury, our results suggest that a low Cx26/Cx43 ratio in adult ependymal cells may be linked to a non-proliferative progenitor phenotype in the intact cord that shifts to a proliferative one with the rise of Cx26 after injury. Similar to injury, the activation of proliferation

induced by P2X7r is paralleled by the re-expression of Cx26<sup>22</sup>. The fact that genetic deletion of Cx26 blocked the effect of P2X7r activation on the induction of proliferation suggests that Cx26 is a fundamental hub for the signalling pathways needed to keep progenitor-like cells of the ependyma in an active state.

Cx26 plays a key role in the development and wound healing of different tissues. For example, selective Cx26 ablation arrests the postnatal development of the organ of Corti<sup>31</sup> and impairs the development of excitatory neocortical neurons<sup>32</sup>. In the normal skin Cx26 expression is very low but between 1 to 4 days after skin injury is upregulated around the wound<sup>14</sup>. Likewise, Cx26 is induced and associated with proliferation in healing of human airway epithelial cell cultures<sup>33</sup>. Our findings support the idea that Cx26 is a key regulator of the proliferation of progenitor-like cells in the ependyma in the context of tissue repair after SCI. Besides proliferation, Cxs have been shown to play a role in cell migration<sup>34</sup> and recently Cx43 has been implied in the migration of ependyma-derived cells<sup>19</sup>. Cx26 expressed in HeLa cells increase the cell motility in scrape wounding models by reducing cell adhesion<sup>35</sup>. It may be possible that Cx26 in ependymal cells are involved in the detachment and migration of ependyma-derived cells. However, the strong interference of Cx26 deletion on injury-induced proliferation precluded to study an eventual role in the migration of ependyma-derived cells. The molecular mechanisms by which Cx26 is upregulated and exert its modulation on proliferation of ependymal cells remain to be explored. Interestingly, during pregnancy Cx26 is strongly upregulated both in mammary epithelial and uterine endometrial cells by transcriptional regulation via SP and AP-2 transcription factors<sup>36,37</sup>. The present study suggests that Cx26 is not the main Cx isoform mediating gap junction coupling in the ependyma. This raises the possibility that the effect of Cx26 on proliferation is mediated by non-canonical functions via the interaction with other proteins. Interestingly, in breast cancer cells Cx26 forms a complex with NANOG and focal adhesion kinase to drive self-renewal<sup>38</sup>. Future studies should explore potential protein interactions with Cx26 to understand the molecular mechanisms by which the cell cycle of ependymal cells is regulated.

The functional role of Cx43 in the healing of different types of epithelia is complex through the regulation of cellular events such as migration and proliferation<sup>39</sup>. The pathological persistence of Cx43 impairs healing<sup>40</sup> whereas blockade of Cx43 improves wound closure in the skin<sup>41</sup> and superficial corneal epithelial wounds<sup>42</sup>. In the SC, Cx43 is strongly expressed in astrocytes and play a role in the spread of tissue damage as its blockade promotes some functional recovery<sup>43,44</sup>. However, our loss-of-function approach showed that instead of an improvement, Cx43 deletion in ependymal cells decreased the reaction of the ependymal stem cell niche to injury. Although we

cannot rule out the interaction of Cx43 or its carboxyterminal with other proteins<sup>45,46</sup>, our data suggests that the effect of Cx43 deletion can be accounted for by the interference of Cx26 upregulation induced by injury. Electrophysiology and dye coupling indicate that Cx43 is the main Cx isoform responsible for the communication between ependymal cells via gap junctions. In addition, in the intact spinal cord there is a subpopulation of functional Cx43 hemichannels<sup>12</sup> and P2X7r<sup>26</sup>. Our data shows that P2X7r activation by BzATP induced Ca<sup>2+</sup> waves that spread within the ependyma, a propagation that depended on Cx signalling as it was blocked by MFA. Both Cx43 hemichannels and gap junctions may play a part in Ca<sup>2+</sup> wave genesis and propagation. As in many other cell types, Cx43 hemichannels may release ATP that would then activate P2X7r in an auto- and paracrine way. The Ca<sup>2+</sup> influx through P2X7r would induce a Ca<sup>2+</sup>-induced Ca<sup>2+</sup> release from the endoplasmic reticulum via ryanodine receptors<sup>26</sup> and permeation of Ca<sup>2+</sup> through gap junctions, leading to the spread of Ca<sup>2+</sup> among a cohort of ependymal cells. The increase in intracellular Ca<sup>2+</sup> would then activate the transcription of Cx26 to reactivate dormant progenitors in the ependyma. Figure 8 shows a cartoon with the proposed cellular mechanisms that imply Cx43 and Cx26 in the reactivation of ependymal cells after injury.

Collectively, our findings show that Cx26 represents an essential hub for the signalling pathways the lead to the resumption of proliferation within the ependymal stem cell niche in response to injury. We propose the main role of Cx43 is -together with P2X7r activation- to initiate a sequence of cellular events by facilitating the spread of Ca<sup>2+</sup> signals, leading to Cx26 upregulation in a cohort of ependymal cells. Cx26 appears as a relevant target to manipulate the ependyma towards a functional state more competent to promote endogenous repair.

## Methods

**Animals.** FoxJ1CreER-R26RtdTomato (kind gift of Prof. Jonas Frisén, Karolinska Institutet)<sup>47</sup> mice were used as control. B6.129S7-Gja1<sup>tm1Dlg/J</sup> (The Jackson Laboratories, RRID:IMSR\_JAX:008039) and B6;129P2-Gjb2<sup>tm1Ugds/Cnrm</sup> (The European Mouse Mutant Archive - EMMA, EM:00245) mice were crossed with FoxJ1CreER-R26RtdTomato (FoxJ1CreER-tdT) mice to selectively delete Cx43 or Cx26 from ependymal cells, respectively. B6.Cg-Gt(ROSA)26Sor<sup>tm38(CAG-GCaMP3)Hze/J</sup> (The Jackson Laboratories, RRID:IMSR\_JAX:029043) mice were crossed with FoxJ1CreER to express the fluorescent calcium indicator protein GCaMP3 selectively in ependymal cells. To induce Cre dependent recombination in adult mice (P>90), we injected Tamoxifen (Sigma; 2 mg, 20 mg/ml in corn oil, i.p.) for 5 days and allowed at least 10 days between the last injection and surgery to ensure clearance<sup>47</sup>. For neonatal mice, two injections of tamoxifen were applied at P9-10 and processed at P11. Male and female animals were used indistinctly. All experimental procedures were approved by our local Committee for Animal Care (protocol #005/09/2015).

**Spinal cord injury (SCI).** Animals were anesthetized using isoflurane (3% for induction, 1-1,5% for maintenance, Terrel<sup>TM</sup>). Injury of the dorsal aspect of the SC was performed as described elsewhere<sup>4,12</sup>. Briefly, after laminectomy the dorsal funiculus at low thoracic level (T13) was cut transversely with microsurgical scissors (depth ~0.8 mm) and the lesion was extended rostrally to comprise about one spinal cord segment. Tramadol (3 mg/kg, i.p) was administered for pain relief immediately after surgery. A second dose of tramadol was applied 24 h after surgery.

**In vivo activation of P2X7 receptors (P2X7r).** Intraspinal injection of the selective P2X7r agonist BzATP (1 µl, 1 mM in saline) was performed as described elsewhere<sup>22</sup>. Briefly, the injection was performed with a glass micropipette (~40 µm tip) pulled from graduated glass capillaries (GC-3.5, RWD Life Sciences). The glass micropipette was secured in a microinjector (RWD life Sciences, R-480 Nanoliter Microinjection Pump) attached to a stereotaxic holder. The pipette was lowered 550 µm lateral from the midline to a depth of 700 µm to be nearby the ependyma without inducing a mechanical damage. The drug was injected at a speed of 0.1 µl/min and the retention time was set in 10 min. After the injection, the pipette was withdrawn in 100 µm steps at 15 s intervals.

**Proliferation assay.** A proliferation assay was done as previously described<sup>12,22</sup>. Briefly, EdU (40 mg/kg, i.p.; Biosynth Ltd.) was injected twice daily (4 h interval) from day 3 to day 5 after BzATP injection or SCI. Animals were sedated with diazepam (10 mg/kg, i.p.) and anesthetized with ketamine (100 mg/kg, i.p) and xylazine (10 mg/kg, i.p.) to be perfused with 4% paraformaldehyde

in 0.1 M phosphate buffer (PB, pH 7.4). EdU labelling was revealed by using the Click-iT Alexa Fluor 647 imaging kit (Invitrogen, Thermo Fisher Scientific).

**Slice preparation and electrophysiology.** Neonatal or adult mice were anesthetized with isoflurane (Terrel™). Immediately after achieving full unresponsiveness to painful stimuli, mice were decapitated and the low thoracic-upper lumbar spinal cord dissected out under cutting Ringer's solution. For neonatal animals the cutting Ringer's solution had the following composition (in mM): NaCl, 101; KCl, 3.8; MgCl<sub>2</sub>, 18.7; CaCl<sub>2</sub>, 1; MgSO<sub>4</sub>, 1.3; HEPES, 10; KH<sub>2</sub>PO<sub>4</sub>, 1.2 and glucose, 25; saturated with 5% CO<sub>2</sub> and 95% O<sub>2</sub> (pH 7.4). Transverse 300 μm slices of the thoraco-lumbar spinal cord were made. For patch clamp recordings, slices were placed in a chamber and superfused at 1 ml min<sup>-1</sup> with Ringer's solution (in mM: NaCl, 124; KCl, 2.4; NaHCO<sub>3</sub>, 26; CaCl<sub>2</sub>, 2.4; MgSO<sub>4</sub>.6H<sub>2</sub>O, 1.3; HEPES, 1.25; KH<sub>2</sub>PO<sub>4</sub>, 1.2; and glucose, 10; saturated with 5% CO<sub>2</sub> and 95% O<sub>2</sub>, pH 7.4). All experiments were performed at room temperature (22°-24°C). Cells were visualized with differential interference contrast optics (Leica Microsystems, DM LFS) or oblique illumination (Olympus, BX51WI) and patch-clamp whole-cell recordings obtained with electrodes filled with (in mM): K-gluconate, 122; Na<sub>2</sub>-ATP, 5; MgCl<sub>2</sub>, 2.5; CaCl<sub>2</sub>, 0.003; EGTA, 1; Mg-gluconate, 5.6; K-HEPES, 5; H-HEPES, 5; and biocytin, 10; pH 7.3, 5–10 MΩ). To visualize recorded cells in living slices, Alexa488 or -594 hydrazide (500 mM, Invitrogen) was added to the pipette solution. Voltage-clamp recordings were performed with a Multiclamp 700B amplifier using pClamp10 (Molecular Devices) or a HEKA amplifier (EPC10 USB) using Patchmaster. Seal resistances were between 1 and 4 GΩ. In voltage-clamp mode, cells were held at -70 mV and the resting membrane potential (RMP) was estimated from the current-voltage relationship (at I = 0). The input resistance was calculated around the RMP.

**Morphological identification of patch-clamp recorded cells.** During whole-cell patch-clamp recordings, cells were filled with biocytin. After completion of the recording period (15 to 30 min), slices were fixed by immersion in 4% PFA in 0.1M phosphate buffer (PB, pH 7.4) overnight. Following PB rinsing, the slices were incubated in PB containing 0.3% Triton X-100 with streptavidin-Alexa488 or -546 (1:200; Invitrogen, Thermo Fisher Scientific), mounted in Prolong (Invitrogen) and imaged in a confocal microscope (Carl Zeiss, LSM800 Airyscan).

**Ca<sup>2+</sup> imaging.** To visualize calcium dynamics FoxJ1CreER mice were crossed with 6.Cg-Gt(ROSA)26Sortm38(CAG-GcaMP3)Hze/J mice (JAX #014538). Recombination was induced with tamoxifen, and imaging performed 14 days after. To make slices from adult animals (300 μm thickness), we used the following cutting Ringer's solution (in mM): NMDG, 92; KCl, 2.5;

NaH<sub>2</sub>PO<sub>4</sub>, 1.5; NaHCO<sub>3</sub>, 30; HEPES, 20; glucose, 25; thiourea, 2; Na- ascorbate, 5; Na-pyruvate, 3; CaCl<sub>2</sub>, 0.5; MgSO<sub>4</sub>, 10; saturated with 5% CO<sub>2</sub> and 95% O<sub>2</sub> (pH 7.4). The slices were incubated for 15 min at 34°C in the same cutting Ringer's solution and then transferred to normal Ringer's solution. Slices were separated into 4 groups that contained either normal Ringer's solution (control), meclofenamic acid (MFA, 100 μM), TAT-Gap19 (200 μM) or TAT-Gap19 scrambled peptide (200 μM). Ca<sup>2+</sup> transients were evoked by focal puff application of BzATP (250-500 μM, 1-3 s duration). Time-lapse imaging (5-20 Hz) was performed using either a LucaR or an iXon EMCCD (Andor) camera using Imaging Workbench 6.0 (INDEC BioSystems) or SOLIS 4.31 (Oxford Instruments) software, respectively. Regions of interest (ROI) were manually drawn around the central canal in areas exhibiting GCaMP3 fluorescence. For each ROI the background-corrected fluorescence  $F$  was calculated as the mean pixel intensity (mean pixel value ROI (t) - mean pixel value ROI background (t)). Baseline fluorescence  $F_0$  was defined as the average  $F$  within 3 seconds before the BzATP application.  $\Delta F/F_0$  was calculated for each ROI as  $(F - F_0)/F_0$ . For event (peak) detection, a responsive ROI was defined as that displaying an event exceeding a threshold of  $F_0 + 8SD (F_0)$ . To evaluate the propagation of the Ca<sup>2+</sup> wave within the ependyma, the ratio of the responsive number of ROI that crossed the threshold over the total number of ROI (# responsive ROI/total # ROI) was calculated for every slice. The maximum  $\Delta F/F_0$  value for each ROI was also calculated. Analysis of the time-lapse images for ROI determination and measurement was performed using FIJI<sup>48</sup>. Background correction,  $\Delta F/F_0$  calculation and peak detection were performed using a custom R script ([https://codeberg.org/M\\_Vidal/Ca2plus\\_imag\\_analysis/src/branch/main/r\\_script\\_ca2+\\_imag.R](https://codeberg.org/M_Vidal/Ca2plus_imag_analysis/src/branch/main/r_script_ca2+_imag.R)).

**Immunohistochemistry.** Animals were anesthetized with ketamine (100 mg/kg, i.p.), xylazine (10 mg/kg, i.p.) and diazepam (10 mg/kg, i.p.) and fixed by intracardiac perfusion with 4% paraformaldehyde in 0.1 M PB. The spinal cord was sectioned with a vibrating microtome (60–80 μm thick), washed twice in PBS and then incubated with primary antibodies in PBS with 0.3% Triton X-100 (Sigma- Aldrich). Sections were then incubated in secondary antibodies conjugated with different fluorophores. Nuclei were stained with DAPI (Invitrogen). Control experiments were performed omitting primary antibodies.

**Experimental design and statistical analyses.** Mice of either sex were randomly assigned to experimental groups. When using injured mice, we checked that loss of weight at sacrifice did not exceed 15%. All images obtained for quantitative analysis were taken using the same pre-set parameters and analysed with Fiji. For quantitative analysis of immunofluorescence data, a minimum of 5 sections were analysed and averaged per biological replicate (3–5 animals for each

experimental condition, unless otherwise stated). To analyse changes in the expression of Cx26 and Cx43, the immunoreactive puncta were converted into particles using a macro developed in IJ1macro language and quantified in the area occupied by tdT within the injection (BzATP or vehicle) or lesion site ( $\pm 250 \mu\text{m}$ , in  $70 \mu\text{m}$  transverse sections). The confocal images were acquired with a LSM800 Zeiss Airyscan confocal microscope. The cross-sectional area around the lesion site was measured and normalized relative to the area of the most proximal intact spinal cord. Statistical analyses were performed with Graphpad prism 9.50.0 with statistical significance set at  $p < 0.05$ . The statistical test chosen for each experiment is noted next to the corresponding result. Numerical values are reported as mean  $\pm$ SD.

## References

1. Courtine, G. & Sofroniew, M. V. Spinal cord repair: advances in biology and technology. *Nat Med* **25**, 898–908 (2019).
2. Becker, C. G. & Becker, T. Adult zebrafish as a model for successful central nervous system regeneration. *Restor Neurol Neurosci* **26**, 71–80 (2008).
3. Mothe, A. J. & Tator, C. H. Proliferation, migration, and differentiation of endogenous ependymal region stem/progenitor cells following minimal spinal cord injury in the adult rat. *Neuroscience* **131**, 177–187 (2005).
4. Meletis, K. *et al.* Spinal cord injury reveals multilineage differentiation of ependymal cells. *PLoS Biol* **6**, e182 (2008).
5. Stenudd, M., Sabelström, H. & Frisén, J. Role of endogenous neural stem cells in spinal cord injury and repair. *JAMA Neurol* **72**, 235–237 (2015).
6. Swayne, L. A. & Bennett, S. A. L. Connexins and pannexins in neuronal development and adult neurogenesis. *BMC Cell Biol* **17**, S10 (2016).
7. Bittman, K. S. & LoTurco, J. J. Differential regulation of connexin 26 and 43 in murine neocortical precursors. *Cereb Cortex* **9**, 188–195 (1999).
8. Nadarajah, B., Jones, A. M., Evans, W. H. & Parnavelas, J. G. Differential expression of connexins during neocortical development and neuronal circuit formation. *J Neurosci* **17**, 3096–3111 (1997).
9. Kunze, A. *et al.* Connexin expression by radial glia-like cells is required for neurogenesis in the adult dentate gyrus. *Proc Natl Acad Sci U S A* **106**, 11336–11341 (2009).
10. Russo, R. E., Reali, C., Radmilovich, M., Fernández, A. & Trujillo-Cenóz, O. Connexin 43 delimits functional domains of neurogenic precursors in the spinal cord. *J Neurosci* **28**, 3298–3309 (2008).

11. Marichal, N., García, G., Radmilovich, M., Trujillo-Cenóz, O. & Russo, R. E. Spatial domains of progenitor-like cells and functional complexity of a stem cell niche in the neonatal rat spinal cord. *Stem Cells* **30**, 2020–2031 (2012).
12. Fabbiani, G. *et al.* Connexin Signaling Is Involved in the Reactivation of a Latent Stem Cell Niche after Spinal Cord Injury. *J Neurosci* **40**, 2246–2258 (2020).
13. Wong, P. *et al.* The Role of Connexins in Wound Healing and Repair: Novel Therapeutic Approaches. *Front. Physiol.* **7**, (2016).
14. Coutinho, P., Qiu, C., Frank, S., Tamber, K. & Becker, D. Dynamic changes in connexin expression correlate with key events in the wound healing process. *Cell Biol Int* **27**, 525–541 (2003).
15. Qiu, C. *et al.* Targeting connexin43 expression accelerates the rate of wound repair. *Curr Biol* **13**, 1697–1703 (2003).
16. Ostrowski, L. E., Hutchins, J. R., Zakel, K. & O'Neal, W. K. Targeting expression of a transgene to the airway surface epithelium using a ciliated cell-specific promoter. *Mol Ther* **8**, 637–645 (2003).
17. Corns, L. F. *et al.* Cholinergic Enhancement of Cell Proliferation in the Postnatal Neurogenic Niche of the Mammalian Spinal Cord. *Stem Cells* **33**, 2864–2876 (2015).
18. New, L. E., Yanagawa, Y., McConkey, G. A., Deuchars, J. & Deuchars, S. A. GABAergic regulation of cell proliferation within the adult mouse spinal cord. *Neuropharmacology* **223**, 109326 (2023).
19. Hachem, L. D. *et al.* Augmenting AMPA receptor signaling after spinal cord injury increases ependymal-derived neural stem/progenitor cell migration and promotes functional recovery. *Nat Neurosci* **28**, 2054–2066 (2025).
20. Yue, W. W. S., Touhara, K. K., Toma, K., Duan, X. & Julius, D. Endogenous opioid signalling regulates spinal ependymal cell proliferation. *Nature* **634**, 407–414 (2024).

21. Wang, X. *et al.* P2X7 receptor inhibition improves recovery after spinal cord injury. *Nat Med* **10**, 821–827 (2004).
22. Falco, M. V. *et al.* P2X7 receptor activation awakes a dormant stem cell niche in the adult spinal cord. *Front. Cell. Neurosci.* **17**, 1288676 (2023).
23. Sabourin, J.-C. *et al.* A mesenchymal-like ZEB1(+) niche harbors dorsal radial glial fibrillary acidic protein-positive stem cells in the spinal cord. *Stem Cells* **27**, 2722–2733 (2009).
24. Ehrlich, H. P. A Snapshot of Direct Cell–Cell Communications in Wound Healing and Scarring. *Advances in Wound Care* **2**, 113–121 (2013).
25. Sabelström, H. *et al.* Resident neural stem cells restrict tissue damage and neuronal loss after spinal cord injury in mice. *Science* **342**, 637–640 (2013).
26. Marichal, N., Fabbiani, G., Trujillo-Cenóz, O. & Russo, R. E. Purinergic signalling in a latent stem cell niche of the rat spinal cord. *Purinergic Signal* **12**, 331–341 (2016).
27. Ngezahayo, A. & Ruhe, F. A. Connexins in the development and physiology of stem cells. *Tissue Barriers* **9**, 1949242 (2021).
28. Rehermann, M. I., Marichal, N., Russo, R. E. & Trujillo-Cenóz, O. Neural reconnection in the transected spinal cord of the freshwater turtle *Trachemys dorbignyi*. *J Comp Neurol* **515**, 197–214 (2009).
29. Bittman, K., Owens, D. F., Kriegstein, A. R. & LoTurco, J. J. Cell coupling and uncoupling in the ventricular zone of developing neocortex. *J Neurosci* **17**, 7037–7044 (1997).
30. Malmersjö, S. *et al.* Neural progenitors organize in small-world networks to promote cell proliferation. *Proc Natl Acad Sci U S A* **110**, E1524-1532 (2013).
31. Wang, Y. *et al.* Targeted connexin26 ablation arrests postnatal development of the organ of Corti. *Biochemical and Biophysical Research Communications* **385**, 33–37 (2009).
32. Su, X. *et al.* Neonatal CX26 removal impairs neocortical development and leads to elevated anxiety. *Proc Natl Acad Sci U S A* **114**, 3228–3233 (2017).

33. Crespin, S. *et al.* Cx26 regulates proliferation of repairing basal airway epithelial cells. *The International Journal of Biochemistry & Cell Biology* **52**, 152–160 (2014).
34. Elias, L. A. B. & Kriegstein, A. R. Gap junctions: multifaceted regulators of embryonic cortical development. *Trends in Neurosciences* **31**, 243–250 (2008).
35. Polusani, S. R., Kalmykov, E. A., Chandrasekhar, A., Zucker, S. N. & Nicholson, B. J. Cell coupling mediated by connexin 26 selectively contributes to reduced adhesivity and increased migration. *Journal of Cell Science* **129**, 4399–4410 (2016).
36. Tu, Z. J., Kollander, R. & Kiang, D. T. Differential Up-Regulation of Gap Junction Connexin 26 Gene in Mammary and Uterine Tissues: The Role of Sp Transcription Factors. *Molecular Endocrinology* **12**, 1931–1938 (1998).
37. Tu, Z. J., Pan, W., Gong, Z. & Kiang, D. T. Involving AP-2 transcription factor in connexin 26 up-regulation during pregnancy and lactation. *Molecular Reproduction Devel* **59**, 17–24 (2001).
38. Thiagarajan, P. S. *et al.* Cx26 drives self-renewal in triple-negative breast cancer via interaction with NANOG and focal adhesion kinase. *Nat Commun* **9**, 578 (2018).
39. Faniku, C. *et al.* The Connexin Mimetic Peptide Gap27 and Cx43-Knockdown Reveal Differential Roles for Connexin43 in Wound Closure Events in Skin Model Systems. *IJMS* **19**, 604 (2018).
40. Brandner, J. M., Houdek, P., Hüsing, B., Kaiser, C. & Moll, I. Connexins 26, 30, and 43: Differences Among Spontaneous, Chronic, and Accelerated Human Wound Healing. *Journal of Investigative Dermatology* **122**, 1310–1320 (2004).
41. Montgomery, J., Ghatnekar, G. S., Grek, C. L., Moyer, K. E. & Gourdie, R. G. Connexin 43-Based Therapeutics for Dermal Wound Healing. *IJMS* **19**, 1778 (2018).
42. Elbadawy, H. M. *et al.* Effect of connexin 43 inhibition by the mimetic peptide Gap27 on corneal wound healing, inflammation and neovascularization. *British J Pharmacology* **173**, 2880–2893 (2016).

43. Cronin, M., Anderson, P. N., Cook, J. E., Green, C. R. & Becker, D. L. Blocking connexin43 expression reduces inflammation and improves functional recovery after spinal cord injury. *Molecular and Cellular Neuroscience* **39**, 152–160 (2008).
44. Tonkin, R. S. *et al.* Gap junction proteins and their role in spinal cord injury. *Front. Mol. Neurosci.* **7**, (2015).
45. Sorgen, P. L., Trease, A. J., Spagnol, G., Delmar, M. & Nielsen, M. S. Protein–Protein Interactions with Connexin 43: Regulation and Function. *IJMS* **19**, 1428 (2018).
46. Leithe, E., Mesnil, M. & Aasen, T. The connexin 43 C-terminus: A tail of many tales. *Biochimica et Biophysica Acta (BBA) - Biomembranes* **1860**, 48–64 (2018).
47. Llorens-Bobadilla, E. *et al.* A latent lineage potential in resident neural stem cells enables spinal cord repair. *Science* **370**, eabb8795 (2020).
48. Schindelin, J. *et al.* Fiji: an open-source platform for biological-image analysis. *Nat Methods* **9**, 676–682 (2012).

## Figure Legends

**Figure 1. Deletion of Cx26 impairs the injury-induced proliferation of ependymal cells.** **a**, genetic strategy to specifically delete Cx26 in adult ependymal cells. **b**, experimental design to analyse the deletion of Cx26 and its impact on the proliferation induced by injury. **c** and **d**, expression of tdT and Cx26 in a FoxJ1CreER-tdT control mouse at 5 DPI, respectively. In this and subsequent figures, the white line delimits the area of tdT expression. **e** and **f**, the expression of Cx26 in the ependyma at 5 DPI is strongly reduced in Cx26<sup>-/-</sup> mice. **g**, box plot showing a significant difference in the number of Cx26 puncta between control and Cx26<sup>-/-</sup> mice ( $p < 0.0001$ , Mann-Whitney U test,  $n = 6$  mice for control and 7 mice for Cx26<sup>-/-</sup>). **h**, EdU<sup>+</sup> nuclei in a control mouse at 5 DPI. **i**, merge of EdU<sup>+</sup> nuclei and DAPI. **j**, EdU uptake at 5 DPI in a Cx26<sup>-/-</sup> mouse. **k**, merge of EdU<sup>+</sup> nuclei and DAPI. **l**, box plot showing a significant difference in the number of Cx26 puncta between control and Cx26<sup>-/-</sup> mice ( $p < 0.0001$ , Mann-Whitney U test,  $n = 3$  mice for control and 7 mice for Cx26<sup>-/-</sup>). In **h** to **k** the white lines show the mask defined by tdT expression where EdU<sup>+</sup> nuclei were counted. Calibration bars: 10  $\mu\text{m}$ .

**Figure 2. Cx26 is needed for the reactivation of the ependyma induced by purinergic signalling.** **a**, experimental design to study the role of P2X7r on the activation of quiescent ependymal cells. **b**, recombined ependymal cells expressing tdT in a FoxJ1CreER-tdT control animal. **c**, BzATP injection in control mice induced a strong proliferative response. **d**, merge of DAPI stained and EdU<sup>+</sup> nuclei. **e-g**, upon deletion of Cx26 in ependymal cells, BzATP injection failed to reactivate proliferation. **h**, spatial profile of the EdU<sup>+</sup> nuclei around the site of BzATP injection. **i**, box plot showing that the number of EdU<sup>+</sup> nuclei in BzATP injected animals was significantly higher in control compared to Cx26<sup>-/-</sup> mice ( $p < 0.0001$ , Mann-Whitney U test,  $n = 3$  mice for each group). Calibration bars: 10  $\mu\text{m}$ .

**Figure 3. Cx43 also plays a role in the awakening of ependymal cells.** **a**, genetic strategy to specifically delete Cx43 in adult ependymal cells. **b**, experimental design to analyse the deletion of Cx43 and its impact on the proliferation induced by injury. **c** and **d**, expression of the reporter gene tdT and Cx43 in a FoxJ1CreER-tdT control mouse, respectively. **e** and **f**, expression of the reporter gene tdT and Cx43 in a Cx43<sup>-/-</sup> mouse, respectively. **g**, box plot showing that the number of Cx43 puncta in the tdT<sup>+</sup> cells is significantly different between control and Cx43<sup>-/-</sup> mice ( $p < 0.01$ ,

Mann-Whitney U test, n=5 mice for each group). **h**, EdU+ nuclei at 5 DPI in a control mouse. **i**, DAPI stained nuclei are overlaid with the EdU+ nuclei shown in **h**. **j**, EdU+ nuclei at 5 DPI in a Cx43<sup>-/-</sup> mouse. **k**, merge of DAPI and EdU+ nuclei shown in **j**. **l**, box plot showing a statistically significant difference (p<0.05, Mann-Whitney U test, n= 3 mice for control and 5 mice Cx43<sup>-/-</sup>) in cell proliferation between the FoxJ1CreER-tdT control and Cx43<sup>-/-</sup> mice. **m** and **n**, tdT expression and immunohistochemistry for Cx26 at 5 DPI in a control mouse, respectively. **o** and **p**, tdT and Cx26 expression at 5 DPI in a Cx43<sup>-/-</sup> mouse, respectively. **q**, box plot showing there is a significant difference (p<0.05, Mann-Whitney U test, n= 5 mice for control and 4 mice for Cx43<sup>-/-</sup>) in the number of Cx26 puncta between control and Cx43<sup>-/-</sup> mice at 5 DPI. Calibration bars: 10 µm.

**Figure 4. The lack of Cx26 in ependymal cells affects scar formation.** **a**, sagittal section of the spinal cord of a FoxJ1CreER-tdT mouse at 30 DPI. The dotted line highlights the outer limit of the cord. **b**, tdT+ cells of a FoxJ1CreER-tdT mouse migrating away from the CC around the lesion epicentre (vertical dotted lines). **c**, box plot of the tdT+ area over the total cross-sectional area of the cord of FoxJ1CreER-tdT mice at 2-, 3- and 4-weeks post injury (WPI). There were no significant differences between selected time points (2 vs. 3 WPI, p> 0.99; 2 vs. 4 WPI, p> 0.99; 3 vs 4 WPI, p>0.99; Kruskal-Wallis Multiple Comparisons test; n= 3 mice for each group). **d** and **e**, representative images of sagittal sections of tdT+ cells around the lesion epicentre in control and Cx26<sup>-/-</sup> mice at 15 DPI, respectively. **f**, tdT+ cells around the lesion epicentre of a Cx43<sup>-/-</sup> mouse. The white dotted lines in **e** to **f** show the dorsal limit of the cord whereas the corresponding 3D reconstructions are shown below each panel. **g**, normalized cross-sectional area of the SC around the lesion epicentre (0) in control (FoxJ1CreER-tdT), Cx26<sup>-/-</sup> and Cx43<sup>-/-</sup> mice. **h**, box plot of the normalized area of the SC around the lesion epicentre (± 250 µm) shows Cx26<sup>-/-</sup> mice have a significantly smaller cross-sectional area of the cord (p<0.05, One Way-ANOVA Dunnett's test) whereas there was no significant difference between control and Cx43<sup>-/-</sup> mice (p=0.53, One Way-ANOVA Dunnett's test, n= 3 mice for each group). Calibration bars: **a**, 1000 µm; **b-f** 100 µm.

**Figure 5. Communication via gap junctions in the active neonatal ependymal stem cell niche.** **a**, currents induced by a family of voltage steps in an ependymal cell of a neonatal FoxJ1CreER-tdT mouse in control medium and after addition of meclofenamic acid (MFA, 100 µM). **b**, current-voltage relationship of data shown in **a**. **c**, paired dot plot showing a significant increase in input resistance induced by MFA (100 µM; p<0.05 Wilcoxon Signed-Rank test), **d** to **f**, representative images of biocytin filled cells recovered after patch-clamp recordings in control, Cx26<sup>-/-</sup> and Cx43<sup>-/-</sup> mice, respectively. In panel **f** two different patch clamp recordings were performed in the same SC slice. **g**, plots showing there was no significant difference between the

input resistance of recorded cells between control and Cx26<sup>-/-</sup> mice ( $p=0.97$ , Mann-Whitney Wilcoxon rank test). However, the input resistance of cells in Cx43<sup>-/-</sup> mice was significantly higher than control ( $p<0.005$ , Mann-Whitney Wilcoxon rank test). **h**, box plot of the volume of dye coupled cells shows that clusters in Cx43<sup>-/-</sup> mice were significantly smaller than control ( $p<0.05$ , Kruskal-Wallis multiple comparison test). There was no significant difference of the volume of dye coupled cells between control and Cx26<sup>-/-</sup> mice ( $p>0.99$ , Kruskal-Wallis multiple comparison tests). Calibration bars: 10  $\mu\text{m}$ .

**Figure 6. Blockade of Cx hemichannels impaired the reaction of ependymal cells to SCI.** **a**, experimental design to explore the role of Cx hemichannels in injury-induced proliferation of ependymal cells. **b**, uptake of EdU in a mouse injected with the scrambled version of TAT-Gap19 at 5 DPI. **c**, DAPI staining overlaid with EdU<sup>+</sup> nuclei show a substantial number of proliferating ependymal cells in the presence of Scr-TAT-Gap19. **d**, blockade of Cx hemichannels with TAT-Gap19 strongly reduced the proliferative reaction to SCI. **e**, merge of DAPI and EdU<sup>+</sup> nuclei shown in **d**. **f**, spatial profile of EdU<sup>+</sup> nuclei around the lesion epicentre. **g**, box plot showing that at 5 DPI the number of EdU<sup>+</sup> nuclei in animals treated with TAT-Gap19 is significantly smaller than those treated with Scr-TAT-Gap19 ( $p<0.0001$ , unpaired t-test). Calibration bars: 10  $\mu\text{m}$ .

**Figure 7. Cx43 hemichannels and gap junctions are needed for Ca<sup>2+</sup> wave propagation within the ependyma.** **a**, differential interference contrast (DIC) image of an adult SC slice showing the ependyma and the position of the puff pipette containing BzATP (1). Pseudo color images of cells expressing GCaMP3 at different time points (2-4). Regions of interest (ROI) used for  $\Delta F/F_0$  are indicated with numbered circles. The scale bar shows the fluorescent values in arbitrary units. **b**, fluorescence ( $\Delta F/F_0$ ) corresponding to each of the ROI shown in **a**. The time of puff application of BzATP is indicated by the magenta bar. Notice that in some locations secondary peaks in fluorescence appeared (asterisks). **c**, the same data shown in **b** but with a faster time-scale to show the onset of the fluorescence increase, which is dramatically different in the different ROI, suggesting that the calcium signal may travel as a wave within the ependyma. **d**, the late component of the calcium wave was eliminated by the gap junction and hemichannel blocker meclofenamic acid (MFA, 100  $\mu\text{M}$ ). **e**, heat map in 13 adjacent ROI showing the dynamic response of the ependyma to BzATP puff application under control conditions and after addition of MFA (100  $\mu\text{M}$ ) to the bath. **f**, paired dot plot of the ratio of cells that responded with a Ca<sup>2+</sup> increase of the total number of cells (responsive ROI/total ROI) shows that MFA (100  $\mu\text{M}$ ) reduced significantly the propagation of the Ca<sup>2+</sup> wave within the ependyma ( $p<0.005$ , Wilcoxon Signed-Rank test). **g**, ratio of cells responding to BzATP in slices incubated in normal Ringer's solution

(control) or MFA (100  $\mu$ M) shows a significant difference in  $\text{Ca}^{2+}$  wave propagation ( $p < 0.005$ , Mann-Whitney U test, 14 slices per group). **h**, maximum  $\Delta F/F_0$  values for individual ROI shows the incubation in MFA (100  $\mu$ M) strongly reduced the intensity of  $\text{Ca}^{2+}$  signals ( $p < 0.0001$  Mann-Whitney U test, 14 slices per group). **i**, ratio of cells responding to BzATP in slices incubated in Scr-TAT-Gap19 (200  $\mu$ M) or TAT-Gap19 (200  $\mu$ M) shows no significant difference in  $\text{Ca}^{2+}$  wave propagation ( $p = 0.5009$ , Mann-Whitney U test). **j**, maximum  $\Delta F/F_0$  values for individual ROI in Scr-TAT-Gap19 and TAT-Gap19 incubated slices shows a statistically significant reduction after the blockade of Cx hemichannels ( $p < 0.0001$ , Mann-Whitney U test, 22 slices per group). Calibration bar: 10  $\mu$ m.

**Figure 8. Cartoon depicting the proposed cellular events leading to reactivation of the ependymal stem cell niche.** Traumatic injury (1) releases ATP -probably with a component accounted by permeation via Cx43 hemichannels (2)- which acts upon P2X7r on ependymal cells inducing  $\text{Ca}^{2+}$  influx (3) that would in turn produce  $\text{Ca}^{2+}$  induced- $\text{Ca}^{2+}$  release from internal stores (4). The increase in cytosolic  $\text{Ca}^{2+}$  may induce ATP release via Cx43 hemichannels (5) that would activate P2X7r on neighbouring ependymal cells leading to the propagation of the  $\text{Ca}^{2+}$  wave within the ependyma via gap junctions (6). The  $\text{Ca}^{2+}$  signal would -among other things- turn on the transcription of Cx26 (7) that favours proliferation, either through its channel properties or by protein-protein interactions (8).

**Extended Data Figure 1. Deletion of Cx26 and Cx43 is specific for ependymal cells.** **a**, strategy for deleting Cx26 or Cx43 specifically in ependymal cells of the adult spinal cord of mice. **b**, schematic drawing showing the regions (squares) where Cx26 immunoreactivity was sampled outside the ependyma. **c**, representative images of immunohistochemical reaction for Cx26 outside the ependyma in control (FoxJ1CreER-tdT) mice at 5 DPI. **d** and **e**, Cx26 immunoreactivity in Cx26<sup>-/-</sup> and Cx43<sup>-/-</sup> mice, respectively. **f**, box plots showing that there were no significant differences in the density of Cx26 puncta outside the ependyma between control versus Cx26<sup>-/-</sup> ( $p = 0.45$ , Kruskal-Wallis multiple comparison test with post hoc Dunn's test), control versus Cx43<sup>-/-</sup> ( $p = 0.91$ , Kruskal-Wallis multiple comparison test with post hoc Dunn's test) and Cx26<sup>-/-</sup> versus Cx43<sup>-/-</sup> ( $p > 0.99$ , Kruskal-Wallis multiple comparison test with post hoc Dunn's test). Calibration bars: 10  $\mu$ m.

**Extended Data Figure 2. Deletion of Cx26 and Cx43 in the active ependymal stem cell niche of neonatal mice.** **a**, genetic strategy to specifically delete Cx26 or Cx43 in ependymal cells of neonatal mice. **b**, schematics of the experimental design. **c**, immunohistochemistry for Cx26 in

FoxJ1CreER-tdT mice. **d**, expression of Cx26 in the ependyma is strongly reduced in Cx26<sup>-/-</sup> neonatal mice. **e**, box plot showing a significant difference in the number of Cx26 puncta between control and Cx26<sup>-/-</sup> mice ( $p < 0.005$ , Mann-Whitney U test). **f**, immunohistochemistry for Cx43 in the ependyma of a control mouse. **g**, in a Cx43<sup>-/-</sup> mouse the number of Cx43 puncta was strongly reduced. **h**, box plot showing a significant difference in the number of Cx43 puncta between control and Cx43<sup>-/-</sup> mice ( $p < 0.01$ , unpaired t-test).

**Extended Data Figure 3. Functional Cx43 hemichannels in ependymal cells of the adult spinal cord.** **a**, EtBr uptake in control mice (FoxJ1CreER-tdT). **b**, overlay of DAPI stained nuclei and the EtBr signal shown in **a**. **c**, EtBr uptake in a Cx43<sup>-/-</sup> mouse. **d**, overlay of DAPI stained nuclei and the EtBr signal shown in **c**. **f**, box plot showing the EtBr uptake in Cx43<sup>-/-</sup> mice is significantly lower than in control mice ( $p < 0.005$ , Mann-Whitney U test,  $n = 3$  for each group). **g**, comparison of the EtBr uptake in recombined (tdT+) and non-recombined (tdT-) in Cx43<sup>-/-</sup> mice ( $p < 0.005$ , Wilcoxon Signed-Rank test).

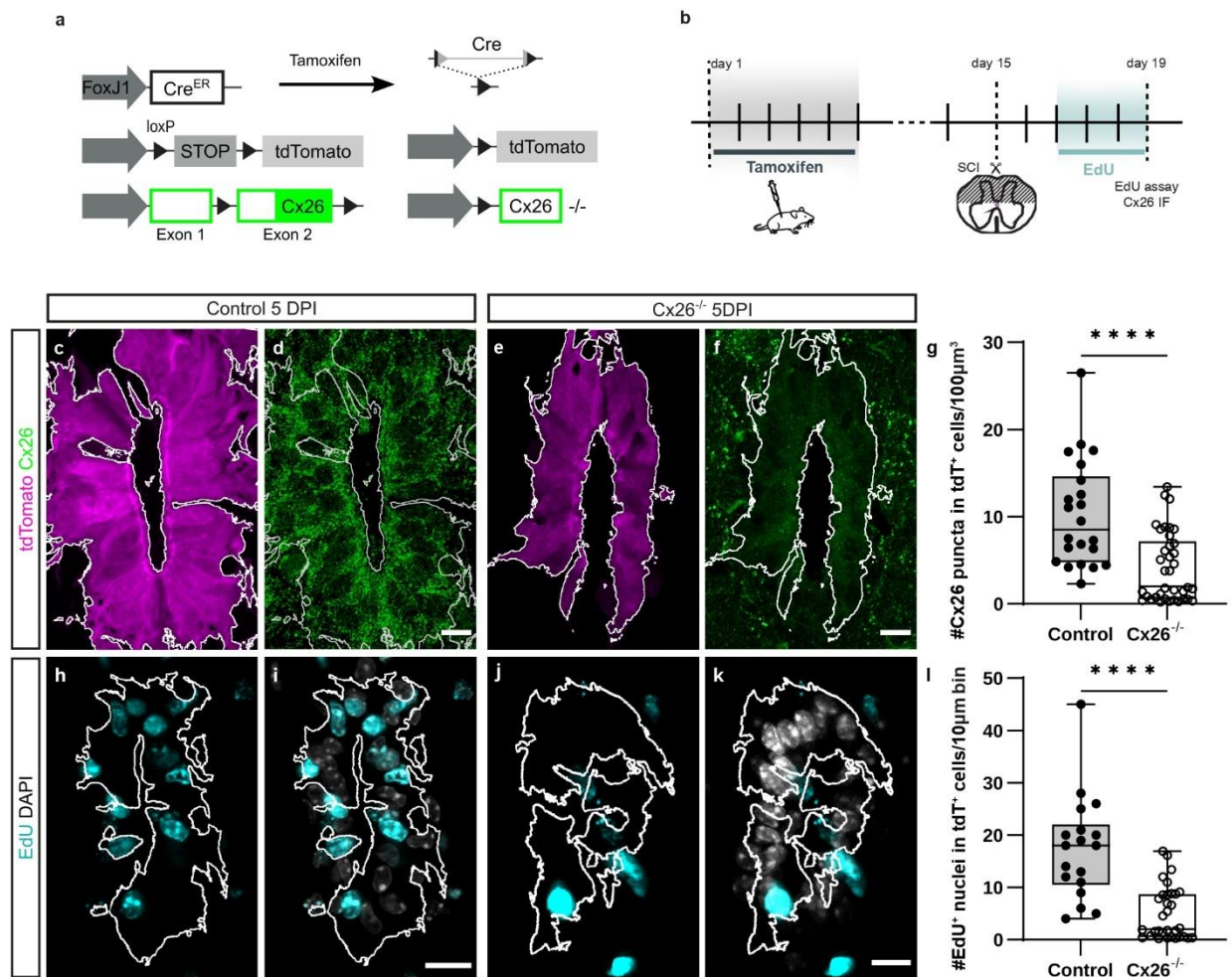


**Figure 1. Deletion of Cx26 impairs the injury-induced proliferation of ependymal cells.** **a**, genetic strategy to specifically delete Cx26 in adult ependymal cells. **b**, experimental design to analyse the deletion of Cx26 and its impact on the proliferation induced by injury. **c** and **d**, expression of tdT and Cx26 in a FoxJ1CreER-tdT control mouse at 5 DPI, respectively. In this and subsequent figures, the white line delimits the area of tdT expression. **e** and **f**, the expression of Cx26 in the ependyma at 5 DPI is strongly reduced in Cx26<sup>-/-</sup> mice. **g**, box plot showing a significant difference in the number of Cx26 puncta between control and Cx26<sup>-/-</sup> mice (p<0.0001, Mann-Whitney U test, n= 6 mice for control and 7 mice for Cx26<sup>-/-</sup>). **h**, EdU+ nuclei in a control mouse at 5 DPI. **i**, merge of EdU+ nuclei and DAPI. **j**, EdU uptake at 5 DPI in a Cx26<sup>-/-</sup> mouse. **k**, merge of EdU+ nuclei and DAPI. **l**, box plot showing a significant difference in the number of Cx26 puncta between control and Cx26<sup>-/-</sup> mice (p<0.0001, Mann-Whitney U test, n= 3 mice for control and 7 mice for Cx26<sup>-/-</sup>). In **h** to **k** the white lines show the mask defined by tdT expression where EdU+ nuclei were counted. Calibration bars: 10 μm.

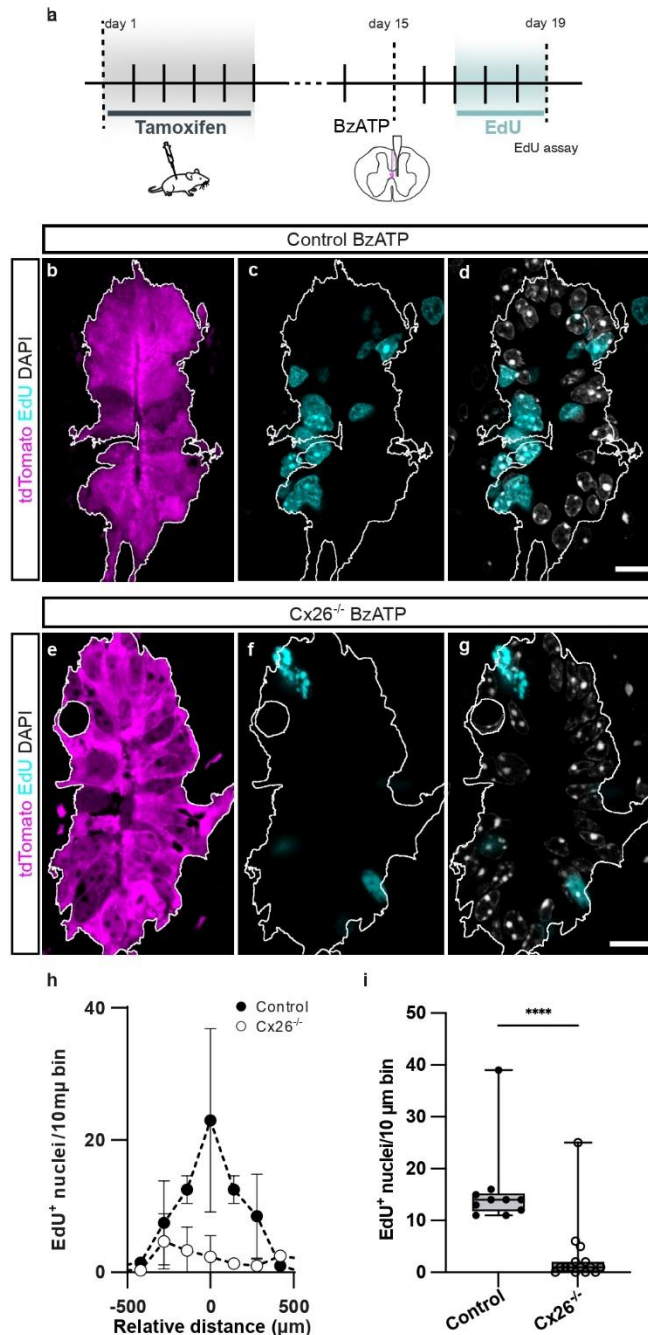


**Figure 2. Cx26 is needed for the reactivation of the ependyma induced by purinergic signalling.** **a**, experimental design to study the role of P2X7r on the activation of quiescent ependymal cells. **b**, recombined ependymal cells expressing tdT in a FoxJ1CreER-tdT control animal. **c**, BzATP injection in control mice induced a strong proliferative response. **d**, merge of DAPI stained and EdU+ nuclei. **e-g**, upon deletion of Cx26 in ependymal cells, BzATP injection failed to reactivate proliferation. **h**, spatial profile of the EdU+ nuclei around the site of BzATP injection. **i**, box plot showing that the number of EdU+ nuclei in BzATP injected animals was significantly higher in control compared to Cx26<sup>-/-</sup> mice ( $p < 0.0001$ , Mann-Whitney U test,  $n = 3$  mice for each group). Calibration bars: 10 μm.

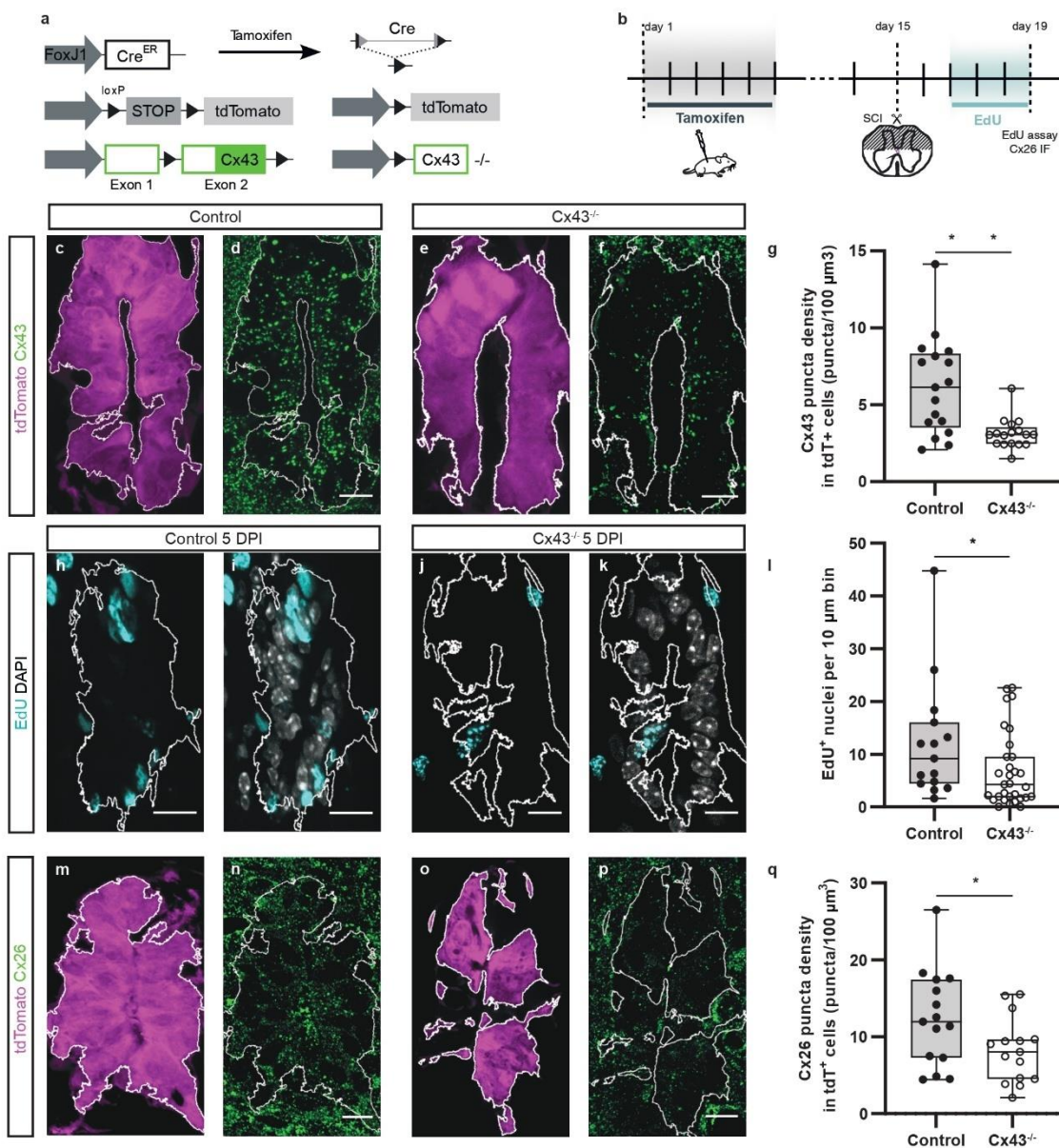


**Figure 3. Cx43 also plays a role in the awakening of ependymal cells.** **a**, genetic strategy to specifically delete Cx43 in adult ependymal cells. **b**, experimental design to analyse the deletion of Cx43 and its impact on the proliferation induced by injury. **c** and **d**, expression of the reporter gene tdT and Cx43 in a FoxJ1CreER-tdT control mouse, respectively. **e** and **f**, expression of the reporter gene tdT and Cx43 in a Cx43<sup>-/-</sup> mouse, respectively. **g**, box plot showing that the number of Cx43 puncta in the tdT<sup>+</sup> cells is significantly different between control and Cx43<sup>-/-</sup> mice (p < 0.01, Mann-Whitney U test, n = 5 mice for each group). **h**, EdU<sup>+</sup> nuclei at 5 DPI in a control mouse. **i**, DAPI stained nuclei are overlaid with the EdU<sup>+</sup> nuclei shown in **h**. **j**, EdU<sup>+</sup> nuclei at 5 DPI in a Cx43<sup>-/-</sup> mouse. **k**, merge of DAPI and EdU<sup>+</sup> nuclei shown in **j**. **l**, box plot showing a statistically significant difference (p < 0.05, Mann-Whitney U test, n = 3 mice for control and 5 mice Cx43<sup>-/-</sup>) in cell proliferation between the FoxJ1CreER-tdT control and Cx43<sup>-/-</sup> mice. **m** and **n**, tdT expression and immunohistochemistry for Cx26 at 5 DPI in a control mouse, respectively. **o** and **p**, tdT and Cx26 expression at 5 DPI in a Cx43<sup>-/-</sup> mouse, respectively. **q**, box plot showing there is a significant

difference ( $p < 0.05$ , Mann-Whitney U test,  $n = 5$  mice for control and 4 mice for Cx43<sup>-/-</sup>) in the number of Cx26 puncta between control and Cx43<sup>-/-</sup> mice at 5 DPI. Calibration bars: 10  $\mu\text{m}$ .

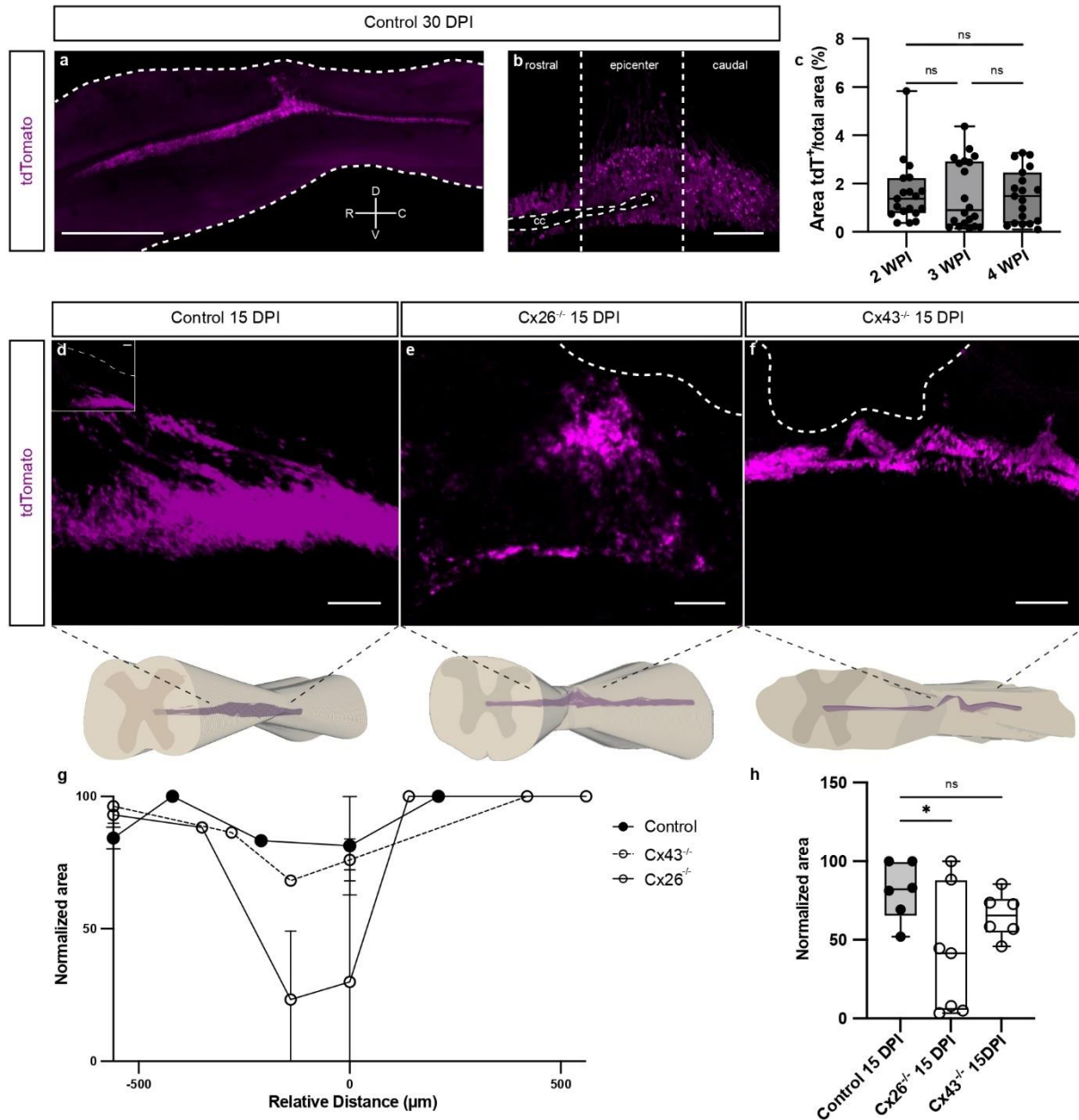


**Figure 4. The lack of Cx26 in ependymal cells affects scar formation.** **a**, sagittal section of the spinal cord of a FoxJ1CreER-tdT mouse at 30 DPI. The dotted line highlights the outer limit of the cord. **b**, tdT+ cells of a FoxJ1CreER-tdT mouse migrating away from the CC around the lesion epicentre (vertical dotted lines). **c**, box plot of the tdT+ area over the total cross-sectional area of the cord of FoxJ1CreER-tdT mice at 2-, 3- and 4-weeks post injury (WPI). There were no significant differences between selected time points (2 vs. 3 WPI,  $p > 0.99$ ; 2 vs. 4 WPI,  $p > 0.99$ ; 3 vs 4 WPI,  $p > 0.99$ ; Kruskal-Wallis Multiple Comparisons test;  $n = 3$  mice for each group). **d** and **e**, representative images of sagittal sections of tdT+ cells around the lesion epicentre in control and Cx26<sup>-/-</sup> mice at 15 DPI, respectively. **f**, tdT+ cells around the lesion epicentre of a Cx43<sup>-/-</sup> mouse. The white dotted lines in **e** to **f** show the dorsal limit of the cord whereas the corresponding 3D reconstructions are shown below each panel. **g**, normalized cross-sectional area of the SC around the lesion epicentre (0) in control (FoxJ1CreER-tdT), Cx26<sup>-/-</sup> and Cx43<sup>-/-</sup> mice. **h**, box plot of the normalized area of the SC around the lesion epicentre ( $\pm 250 \mu\text{m}$ ) shows Cx26<sup>-/-</sup> mice have

a significantly smaller cross-sectional area of the cord ( $p < 0.05$ , One Way-ANOVA Dunnett's test) whereas there was no significant difference between control and Cx43<sup>-/-</sup> mice ( $p = 0.53$ , One Way-ANOVA Dunnett's test,  $n = 3$  mice for each group). Calibration bars: **a**, 1000  $\mu\text{m}$ ; **b-f** 100  $\mu\text{m}$ .

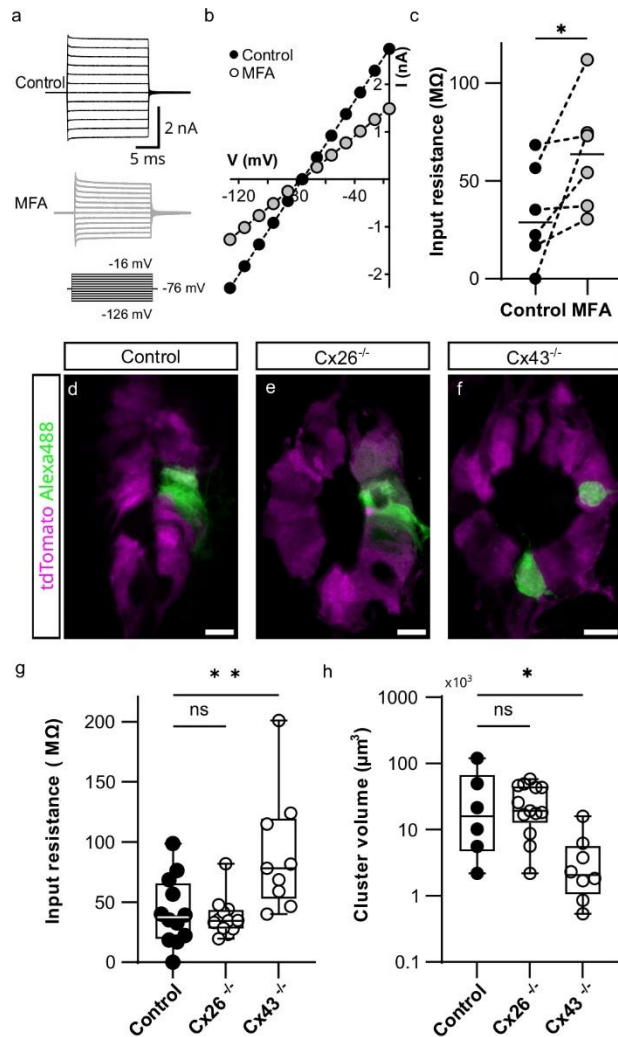


**Figure 5. Communication via gap junctions in the active neonatal ependymal stem cell niche.** **a**, currents induced by a family of voltage steps in an ependymal cell of a neonatal FoxJ1CreER-tdT mouse in control medium and after addition of meclofenamic acid (MFA, 100  $\mu$ M). **b**, current-voltage relationship of data shown in **a**. **c**, paired dot plot showing a significant increase in input resistance induced by MFA (100  $\mu$ M;  $p < 0.05$  Wilcoxon Signed-Rank test), **d** to **f**, representative images of biocytin filled cells recovered after patch-clamp recordings in control, Cx26<sup>-/-</sup> and Cx43<sup>-/-</sup> mice, respectively. In panel **f** two different patch clamp recordings were performed in the same SC slice. **g**, plots showing there was no significant difference between the input resistance of recorded cells between control and Cx26<sup>-/-</sup> mice ( $p = 0.97$ , Mann-Whitney Wilcoxon rank test). However, the input resistance of cells in Cx43<sup>-/-</sup> mice was significantly higher than control ( $p < 0.005$ , Mann-Whitney Wilcoxon rank test). **h**, box plot of the volume of dye coupled cells shows that clusters in Cx43<sup>-/-</sup> mice were significantly smaller than control ( $p < 0.05$ , Kruskal-Wallis multiple comparison test). There was no significant difference of the volume of dye coupled cells between control and Cx26<sup>-/-</sup> mice ( $p > 0.99$ , Kruskal-Wallis multiple comparison tests). Calibration bars: 10  $\mu$ m.

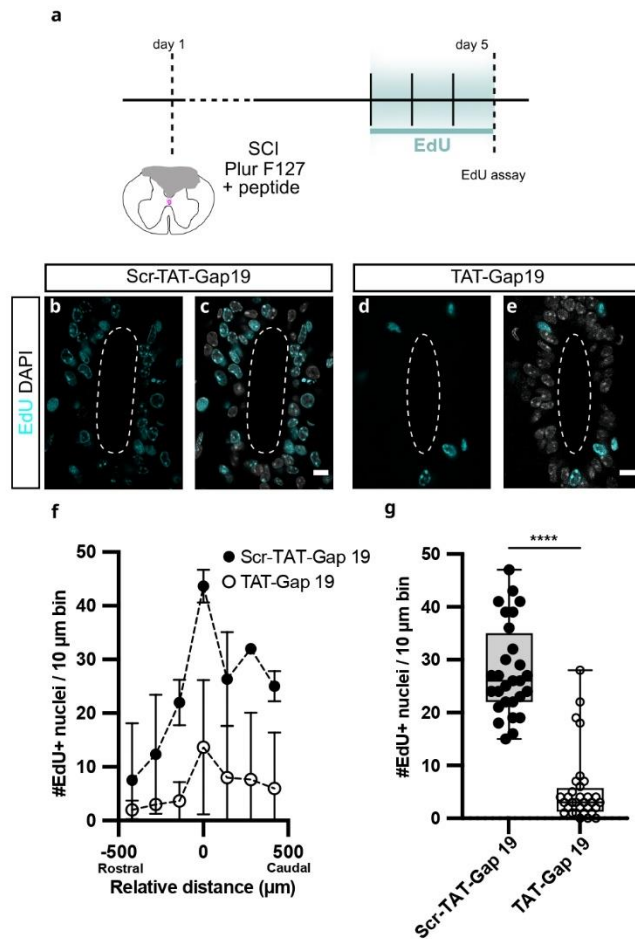


**Figure 6. Blockade of Cx hemichannels impaired the reaction of ependymal cells to SCI.** **a**, experimental design to explore the role of Cx hemichannels in injury-induced proliferation of ependymal cells. **b**, uptake of EdU in a mouse injected with the scrambled version of TAT-Gap19 at 5 DPI. **c**, DAPI staining overlayed with EdU+ nuclei show a substantial number of proliferating ependymal cells in the presence of Scr-TAT-Gap19. **d**, blockade of Cx hemichannels with TAT-Gap19 strongly reduced the proliferative reaction to SCI. **e**, merge of DAPI and EdU+ nuclei shown in **d**. **f**, spatial profile of EdU+ nuclei around the lesion epicentre. **g**, box plot showing that at 5 DPI the number of EdU+ nuclei in animals treated with TAT-Gap19 is significantly smaller than those treated with Scr-TAT-Gap19 ( $p < 0.0001$ , unpaired t-test). Calibration bars: 10  $\mu$ m.

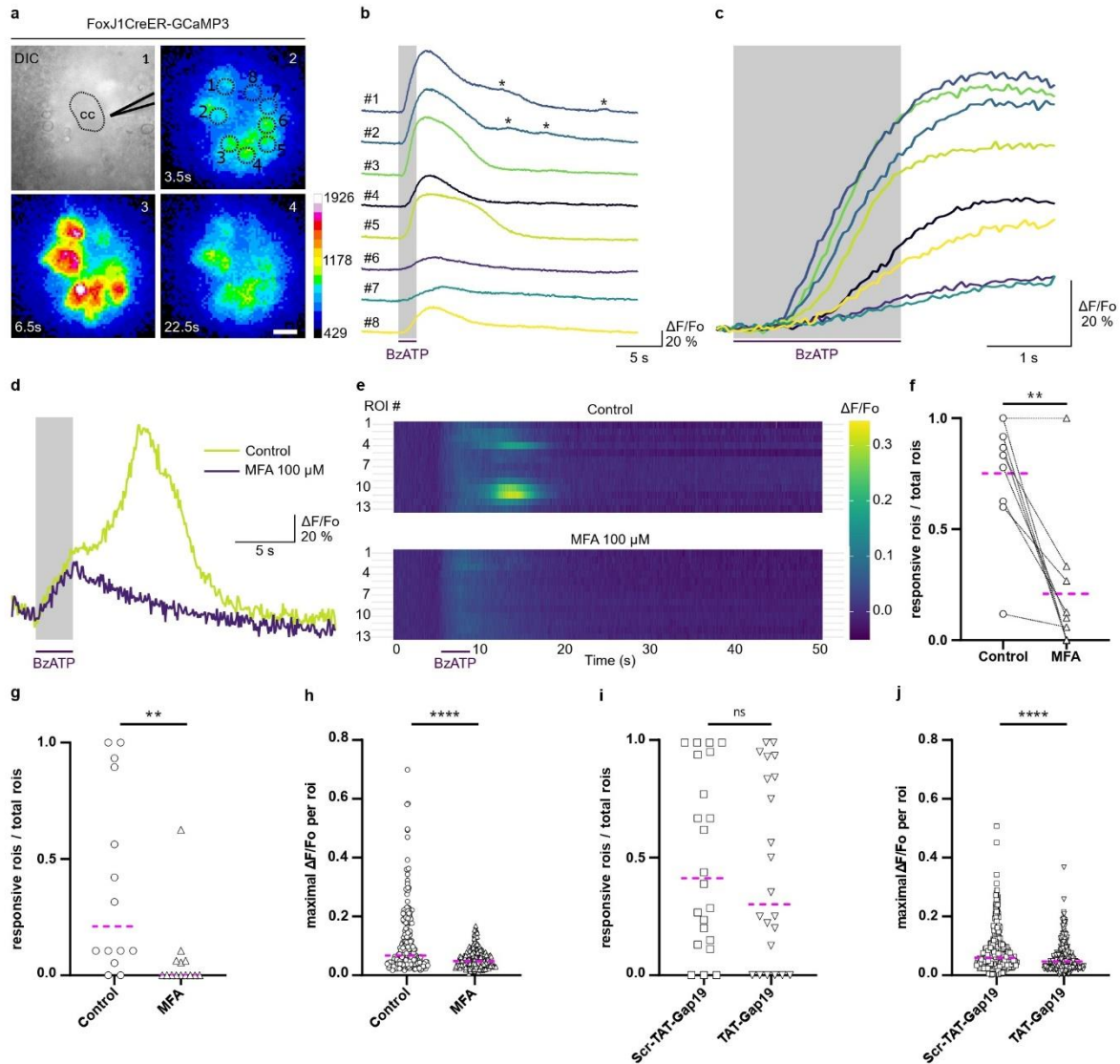


### Figure 7. Cx43 hemichannels and gap junctions are needed for Ca<sup>2+</sup> wave propagation within the ependyma.

**a**, differential interference contrast (DIC) image of an adult SC slice showing the ependyma and the position of the puff pipette containing BzATP (1). Pseudo color images of cells expressing GCaMP3 at different time points (2-4). Regions of interest (ROI) used for  $\Delta F/Fo$  are indicated with numbered circles. The scale bar shows the fluorescent values in arbitrary units. **b**, fluorescence ( $\Delta F/Fo$ ) corresponding to each of the ROI shown in **a**. The time of puff application of BzATP is indicated by the magenta bar. Notice that in some locations secondary peaks in fluorescence appeared (asterisks). **c**, the same data shown in **b** but with a faster time-scale to show the onset of the fluorescence increase, which is dramatically different in the different ROI, suggesting that the calcium signal may travel as a wave within the ependyma. **d**, the late component of the calcium wave was eliminated by the gap junction and hemichannel blocker meclofenamic acid (MFA, 100  $\mu M$ ). **e**, heat map in 13 adjacent ROI showing the dynamic response of the ependyma to BzATP puff application under control conditions and after addition of MFA (100  $\mu M$ ) to the bath. **f**, paired dot plot of the ratio of cells that responded with a Ca<sup>2+</sup> increase of the total number of cells (responsive ROI/total ROI) shows that MFA (100  $\mu M$ ) reduced significantly the propagation of the Ca<sup>2+</sup> wave within the ependyma ( $p < 0.005$ , Wilcoxon Signed-

Rank test). **g**, ratio of cells responding to BzATP in slices incubated in normal Ringer's solution (control) or MFA (100  $\mu$ M) shows a significant difference in  $\text{Ca}^{2+}$  wave propagation ( $p < 0.005$ , Mann-Whitney U test, 14 slices per group). **h**, maximum  $\Delta F/F_0$  values for individual ROI shows the incubation in MFA (100  $\mu$ M) strongly reduced the intensity of  $\text{Ca}^{2+}$  signals ( $p < 0.0001$  Mann-Whitney U test, 14 slices per group). **i**, ratio of cells responding to BzATP in slices incubated in Scr-TAT-Gap19 (200  $\mu$ M) or TAT-Gap19 (200  $\mu$ M) shows no significant difference in  $\text{Ca}^{2+}$  wave propagation ( $p = 0.5009$ , Mann-Whitney U test). **j**, maximum  $\Delta F/F_0$  values for individual ROI in Scr-TAT-Gap19 and TAT-Gap19 incubated slices shows a statistically significant reduction after the blockade of Cx hemichannels ( $p < 0.0001$ , Mann-Whitney U test, 22 slices per group). Calibration bar: 10  $\mu$ m.

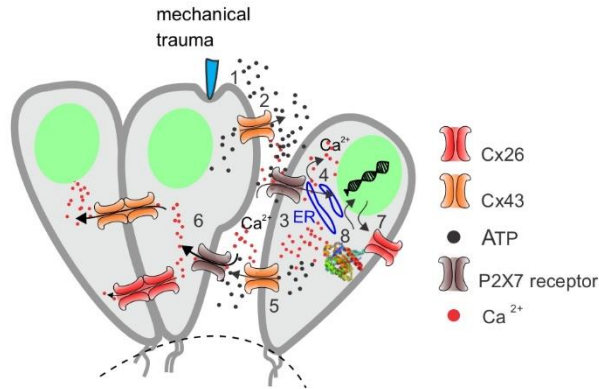
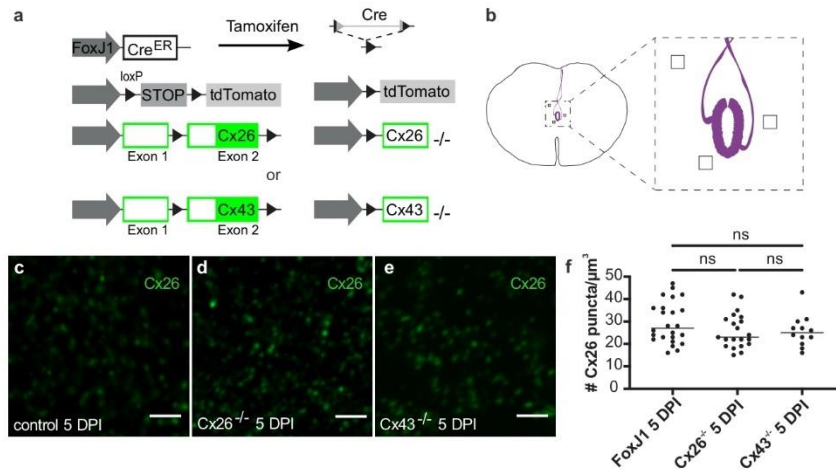
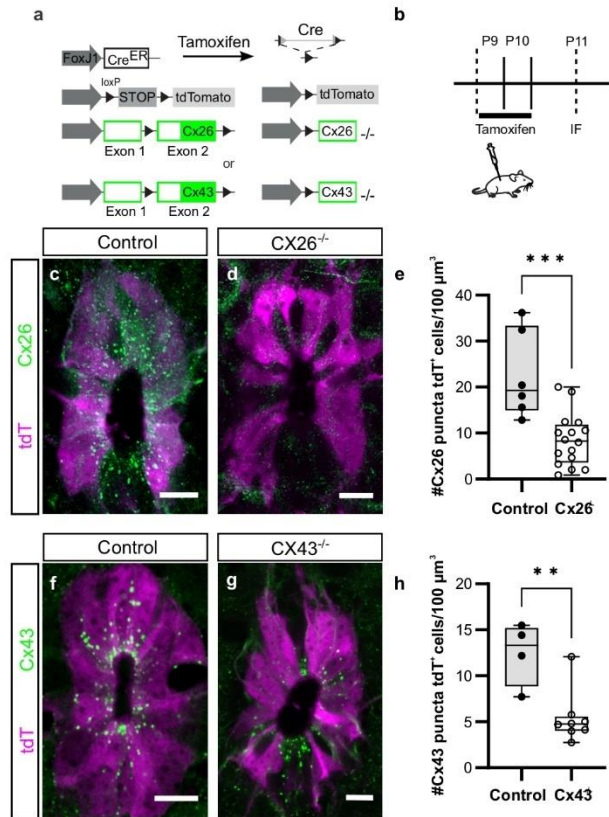


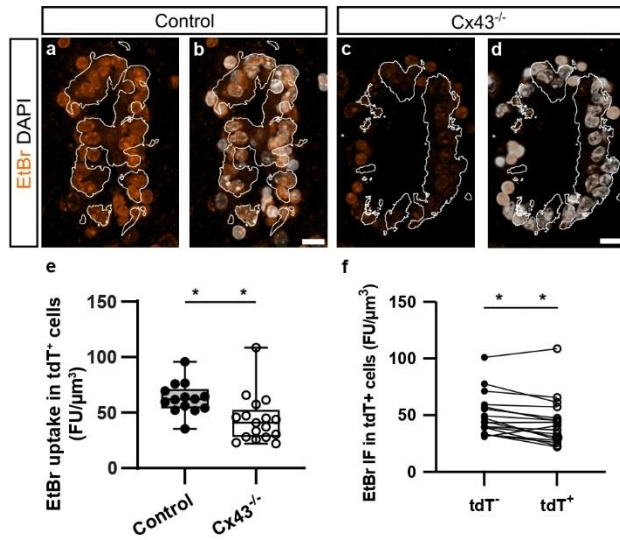
**Figure 8. Cartoon depicting the proposed cellular events leading to reactivation of the ependymal stem cell niche.** Traumatic injury (1) releases ATP -probably with a component accounted by permeation via Cx43 hemichannels (2)- which acts upon P2X7r on ependymal cells inducing  $\text{Ca}^{2+}$  influx (3) that would in turn produce  $\text{Ca}^{2+}$  induced- $\text{Ca}^{2+}$  release from internal stores (4). The increase in cytosolic  $\text{Ca}^{2+}$  may induce ATP release via Cx43 hemichannels (5) that would activate P2X7r on neighbouring ependymal cells leading to the propagation of the  $\text{Ca}^{2+}$  wave within the ependyma via gap junctions (6). The  $\text{Ca}^{2+}$  signal would -among other things- turn on the transcription of Cx26 (7) that favours proliferation, either through its channel properties or by protein-protein interactions (8).



**Extended Data Figure 1. Deletion of Cx26 and Cx43 is specific for ependymal cells.** **a**, strategy for deleting Cx26 or Cx43 specifically in ependymal cells of the adult spinal cord of mice. **b**, schematic drawing showing the regions (squares) where Cx26 immunoreactivity was sampled outside the ependyma. **c**, representative images of immunohistochemical reaction for Cx26 outside the ependyma in control (FoxJ1CreER-tdT) mice at 5 DPI. **d** and **e**, Cx26 immunoreactivity in Cx26<sup>-/-</sup> and Cx43<sup>-/-</sup> mice, respectively. **f**, box plots showing that there were no significant differences in the density of Cx26 puncta outside the ependyma between control versus Cx26<sup>-/-</sup> ( $p = 0.45$ , Kruskal-Wallis multiple comparison test with post hoc Dunn's test), control versus Cx43<sup>-/-</sup> ( $p = 0.91$ , Kruskal-Wallis multiple comparison test with post hoc Dunn's test) and Cx26<sup>-/-</sup> versus Cx43<sup>-/-</sup> ( $p > 0.99$ , Kruskal-Wallis multiple comparison test with post hoc Dunn's test). Calibration bars: 10  $\mu\text{m}$ .



**Extended Data Figure 2. Deletion of Cx26 and Cx43 in the active ependymal stem cell niche of neonatal mice.** **a**, genetic strategy to specifically delete Cx26 or Cx43 in ependymal cells of neonatal mice. **b**, schematics of the experimental design. **c**, immunohistochemistry for Cx26 in FoxJ1CreER-tdT mice. **d**, expression of Cx26 in the ependyma is strongly reduced in Cx26<sup>-/-</sup> neonatal mice. **e**, box plot showing a significant difference in the number of Cx26 puncta between control and Cx26<sup>-/-</sup> mice ( $p < 0.005$ , Mann-Whitney U test). **f**, immunohistochemistry for Cx43 in the ependyma of a control mouse. **g**, in a Cx43<sup>-/-</sup> mouse the number of Cx43 puncta was strongly reduced. **h**, box plot showing a significant difference in the number of Cx43 puncta between control and Cx43<sup>-/-</sup> mice ( $p < 0.01$ , unpaired t-test).



**Extended Data Figure 3. Functional Cx43 hemichannels in ependymal cells of the adult spinal cord.** **a**, EtBr uptake in control mice (FoxJ1CreER-tdT). **b**, overlay of DAPI stained nuclei and the EtBr signal shown in **a**. **c**, EtBr uptake in a  $Cx43^{-/-}$  mouse. **d**, overlay of DAPI stained nuclei and the EtBr signal shown in **c**. **e**, box plot showing the EtBr uptake in  $Cx43^{-/-}$  mice is significantly lower than in control mice ( $p < 0.005$ , Mann-Whitney U test,  $n = 3$  for each group). **f**, comparison of the EtBr uptake in recombined ( $tdT^{+}$ ) and non-recombined ( $tdT^{-}$ ) in  $Cx43^{-/-}$  mice ( $p < 0.005$ , Wilcoxon Signed-Rank test).